ROTATIONAL HEAT CAPACITY OF DIATOMIC MOLECULES IN ATOMIC CRYOCRYSTALS

By
Tilahun Tesfaye

**A Thesis Submitted to
the School of Graduate Studies
Addis Ababa University**

**In Partial Fulfillment of
the Requirements for
the Degree Master of Science in Physics**

June 1992

Dedicated to my father Ato Tesfaye Deressu

and

to my mother Wo/ Zelekash Degefu.

ACKNOWLEDGEMENT

My sincere appereciation and thanks go to my advisor and instructor **Dr. A.M Tolkachev** who suggested the problem and went with me up to the end through all troubles of the research work directng it intelligently until the desired goal is finally achieved.

I acknowledge highly **P.I. Muromtsev, M.I Bagatsky and V.G.Manzhilii of Physicotechnical Institute of Low Temperatures, Acadamy of Sciences of Ukrainian SSR Kharkov** for sending their recent experimental data to be analized here.

I am greatfull to the **Staff of the Computer lab.in the Mathematics department** for allowing me to use the computer facillities there and their assistance during the work.

It is pleasure to express my appreciation of the hospitality rendered to me by my **Sisters Azeb and Tirsit** during the years of my study.

My acknowledgement also goes to the acquisition department of the A.A.U. Library for its kind collaboration in ordering articles not available here from abroad. And at last but not least I would like to express my great indeptedness to **Ato Samuel T/Giorgis** for his help in facilitating the print of the work.

Tilahun Tesfaye.

CONTENTS

CONTENTS (contd.)

ABSTRACT

A Comparative analysis has been carried out between the experimental excess heat capacity of solid solutions of $^{14}N_2$ and $^{15}N_2$ in Ar and Kr due to rotation of the nitrogen molecules, and the existing theoretical models in the temperature range 0.5 t0 6 Kelvin. It is shown that the well known Devonshire-Manz-Mirsky (DMM) model can not explain the observed heat capacity below 2K neither on the basis of the assumption of frozen high-temperature nor equlibrium concentration of different spin nuclear modifications of nitrogen. Splitting of the lowest rotational energy levels of the impurinty molecules is proposed, so as to provide an agreement between the experimental observations and theoretical data. It is also concluded that experimental observations favour the frozen high-temperature composition of the different spin species of nitrogen down to 0.5K in temperature, and the equilibrium orientation of the molecules is along the <100> directions of the crystal.

I. INTRODUCTION

The heat capacity of a given system is very sensitive to the peculiarities of its energy spectrum. The rotation of impurity molecules in a crystal gives rise to a pronounced maxima on the background of the lattice contribution to the heat capacity of the system specifically at low temperatures where the state density and hence the heat capacity of the crystal is very small.

In this work the excess heat capacity of solidified inert gase, Ar and Kr, due to the rotation of homonuclear diatomic impurity molecules namely $^{14}N_2$ and $^{15}N_2$, was studied. The rotation of the impurity molecules is hindered by the crystal field, in effect distorting the energy spectrum of the molecules as well as the symmetry of the crystal field.

One of the motivations for studying hindered rotation in solids is the hope that accurate information about the details ofthe low lying energy spectra of rotating molecules and rotational barriers can be obtained through heat capacity measurements such as are obserbed for CO [1], N_2 [2], LiCl [3] substitutionally trapped in crystals and, CH_4 [4] With in their own matrices. This makes the heat capacity method of investigation as important as other (spectroscopic, NMR, etc) methods of investigating crystal energy spectrum .

The effect of crystalline field on the rotational states of linear molecules is theoretically described in 1936 by Devonshire [5]. In the **Devonshire'model** the energy spectrum of linear molecules is expressed in terms of a parameter **K** characterizing the strength of the crystal field and the rotational constant B of the impurity molecule. The Devonshire model is modified in the 1980's by **Manz** [6], and **Manz-Mirsky** [7], to incorporate lattice relaxations accompanying the introduction of foreign molecules and their rotations. This latter model is referred to as the **Devonshire-Manz-Mirsky (DMM) model.**

Literature shows that the Devonshire-Manz-Mirsky (DMM) model, which assumes an instantaneous spatial adjustement of surrounding atoms to a rotating impurity molecule, provides a satisfactory explantion to the observed experimental excess heat capacity of systems of solidified inert gases with molecular impurities in the temperature region above 2K. The agreement between experimental observations and predictions of the DMM model in this temperature region is not suffient to provide all the informations we seek to taste the adequacy of the energy spectrum of the impurity molecules and the symmetry of the crystal field given by the theory for the reasons mentioned below.

A given isotope of nitrogen molecule exists in two different spin nuclear modifications which occupy even rotational levels for the modification of one type and odd levels for the other. The DMM theory predicts practically the same value of heat capacity above 2k whether we have assumed there exists conversion, or no conversion, between the two modifications. But the theory predicts peaks below 2k which are substantially different in magnitude and in their position with respect to temperature for the two assumptions. This stood as the first information we lack as to the existence of conversion between the two species of nuclear modifications.

Secondly the choices of the parameters B and K, from measurements in the temperature regions so far investigated, are not free from ambiguity for there is an error growing with temperature in the values of rotational heat capacity that are extracted from the measured heat capacity of the solid solutions.

The third reason is that which potential topography of the crystal field (positve or negative value of the parameter K) is favoured by the impurity molecules in relation to the observed experimental data is not evident from high temperature measurements only. In contrast the lower levels of the spectra of hindered rotation show appreciable difference for the two choices of K.

All these reasons show the more informative character of low-temperature experimental results. Thus it is essential to have a comparative analysis between predictions of the theory and low temperature experimental data. To this end I used the recent (Dec.1991) experimental results in the temperature range 0.5 to 6k. These data were obtained from Phisicotecnical institute of low temperatures, acadamy of sciences of Ukrain. Analysis is made on the basis of DMM model, first to test the validity of the model it self and, to answer questions that remain open for the reasons mentioned above.

The low temperature heat capacity of solid solutions:

(a) Ar-$^{14}N_2$, with 0.12, 0.25, 0.5, 1.02, and 2.74 mole% $^{14}N_2$ concentrations,

(b) Ar-$^{15}N_2$, with 0.13, 0.25mole% $^{15}N_2$ concentrations and

(c) Kr-$^{14}N_2$, with 0.131, and 0.25 mole% $^{14}N_2$ concentrations

are analized. As the DMM model neglects the interaction between the impurities, directly or via their respective regions of relaxation, the small amount of concentrations (as compared with the previous works) used in this work are expected to meet the negligible amount of interaction between the impurities required by the theory.

The use of $^{14}N_2$ (nuclei Bose particles) and $^{15}N_2$ (nuclei Fermi particles) as rotating impurities is in view of the possible dependence of the energy spectrum and interconversion

between different species of the molecule on their nuclear spin. Thus the analysis may serve as the ultimate teste of the DMM model.

The low lying energetic levels of molecules being more sensitive to the symmetry of the local field around the impurity, so do the low temperature heat capacity which is predominantly due to transition between these levels. Thus the low temperature heat capacity data is believed to deliver the expected informations up on analysis.

Informations obtained regarding the local structure of crystal from heat capacity measurements may lead to more refined theories of dynamics of impurities in a crystal.

The central theme of this work being a comparative analysis of the theoretical model developed to explain the rotational motion of diatomic molecules substitutionally trapped in atomic crystals as appplied to provide explanations to the observed excess heat capacity of $^{14}N_2$ and $^{15}N_2$ molecules in Ar and Kr matrices, the paper is organized as follows. In chapter I a brief survey of heat capacity dependence on the features of energy spectrum is given. In chapter II the models developed in the theoretical treament and experimental results from literature are compared. The latest experimental results are presented in chapter III, where the comparison with the

existing theory is also made. Experimental discrepancies with the theory are noted and in chapter IV, the necessary modifications to the spectrum in order to resolve these discrepancies, are made. Computer programs used in the data analysis are also included at the end of this thesis.

CHAPTER 1 HEAT CAPACITY DEPENDENCE ON PECULIARITIES OF ENERGY SPECTRUM.

1.1 Heat Capacity Dependence On Energy Spectrum of Particles.

Low temperature measurement of heat capacities of solids, has very sharp dependence on the details of the energy spectrum. In ideal crystals, the constituent atoms or molecules undergo (either through thermal agitation or quantum mechanical zeropoint enery) small oscillations about their equilibrium positions. The oscillators are viewed as coupled which can be decomposed in to the crystal's independent 3N normal mode frequencies. The internal energy of the crystal due to these vibrational degrees of freedom is:

$$E=\sum h\nu_i\left(\frac{1}{2}+\frac{1}{(\exp\theta_i-1)}\right) \qquad \ldots(1.1)$$

and the heat capacity associated with the vibrational degrees of freedom is thus

$$C_v=k\sum \frac{(\theta_i/kT)^2}{(\sinh^2\theta_i/2)} \qquad \ldots(1.2)$$

where $\theta_i = h\nu_i/kT$.

Generally as the number of degrees of freedom become infinite, the normal mode frequencies become so dense that a frequency distribution g(ν) exists with a property such that the number of frequencies less than the frequency ν is

$$\int_0^{\nu} \nu g(\nu)\, d\nu$$

The heat capacity can be expressed as an integral with respect to the frequency ν :

$$C_v = k\int_0^{\nu_m} g(\nu)\, \frac{(h\nu/2kT)^2}{\sinh^2(h\nu/2kT)}\, d\nu \qquad \ldots(1.3)$$

where ν_m is the largest normal mode frequency.

The central problem for early theoreticians was detrmination of g(ν).

Einstein in 1907 [8], pointed out that, owing to the quantization of energy, the law of equipartition must break down at low temperatures and he treated the solid as a system of simple harmonic oscillators of the same frequency, attributing to

the motion of each atom the energy 3h ν /{exp(h ν /kT)-1}. The atomic heat capacity thus becomes temperature dependent and of the form equation 1.4a.

A few years latter Nernest and Lindeman have shown that if

$$C_v = 3K(h\nu/kT)^2 \frac{(h\nu/kT)^2}{(\exp\frac{h\nu}{kT}-1)^2} \qquad \ldots(1.4a)$$

instead of one, two frequencies ν and ν /2 were introduced agreement with the experimental results was rather better.

Experimental works at lower temperatures (liquid He and H) however demonstrated that in this region the specific heats fell not nearly so steeply as predicated by equation (1-4a). This is not surprising since the model used by Einstein makes no provision for the vibrations of lower frequencies in the energy spectrum of the solid which will be preferentially excited in the region of small energy, i.e low temperature.

Debye treated the solid as a continuum in which the thermal vibrations are represented by all possible modes of standing waves, ranging from acoustic vibrations up to a limiting

spectra Fig 1-1,d which differs considerably from the simple parabolic for the isotropic medium. the actual spectra coinicide with Debye's approximation in the regions of lowest frequencies but then rise much steeper to complicated form, exhibiting generally two maxima. Comparison of Fig. 1-1,b and d makes it clear why the simple Nernst-Lindemann approximation was relatively successful, except at the lowest temperatures.

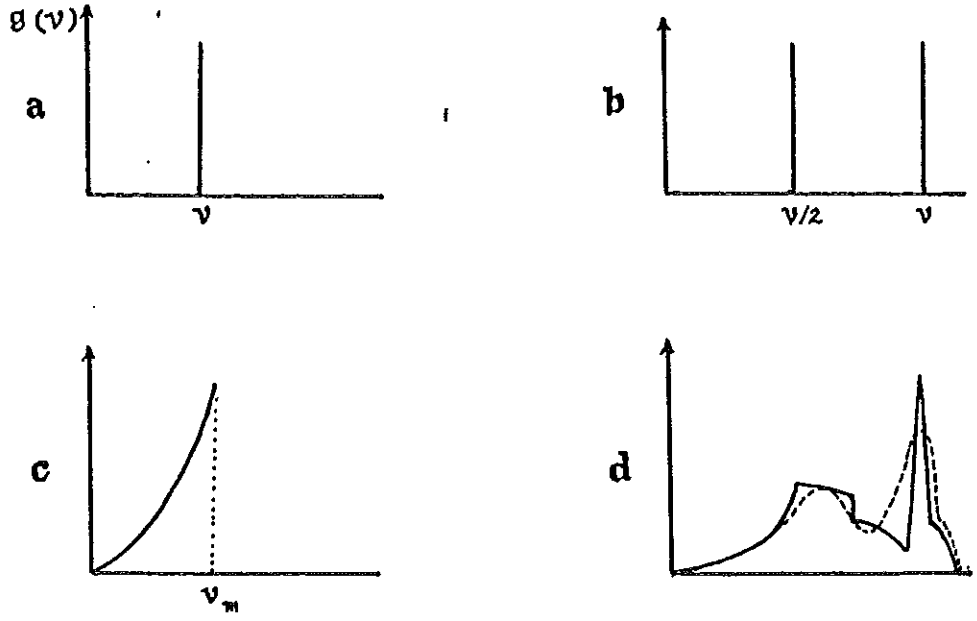

Fig 1.1 Frequency spectrum of a solid according to
(a) Einstein, (b) Nernst-Lindeman, (c) Debye,
(d) _ _ _ _ Blackman, ——— actual distribution from ref.13.

1.1.1 Heat capacity anomalies

Energy taken up by a solid is not all expended on exciting thermal vibrations of the lattice. If there are internal degrees of freedom giving rise to discret quantized energy states quite separate from the spectrum of levels arising from the collective

motion of the lattice, they must make themselves felt in the heat capacity of the solid.

The contributions to the heat capacity of such levels, which are observed over a limited temperature range are observed as bumps or pronounced peaks on the background of the lattice contribution at low temperatures where the lattice heat capacity is very small. These bumps or peaks are referred to as specific heat anomalies. Such internal states may arise in a phenomena as diverse as molecular rotation, crystalline field interaction with paramagnetic ions, and nuclear hyperfine structure splittings provided the thermal population of the energy levels is independent of neighboring atoms. Order-disorder transitions also cause cooperative anomaly.

The most common type of heat capacity anomaly is the one arising from an independent two level system: a ground state and one excited state Δ E above the ground state. The levels of a two level system are populated according to the simple Boltzmann statistics and the additional term in the specific heat resulting from increasing the population of the higher levels is given

$$\Delta C\text{-}Nk\left(\frac{\Delta E}{kT}\right)^2 \frac{g_o}{g_1}\left[1+\frac{g_o}{g_1}\exp\left(\frac{\Delta E}{kT}\right)\right]^{-2} \qquad \ldots(1.5)$$

where N is total number of two level systems in the sample, g_o and g_1 are degeneracies of the ground and the first excited levels respectively.

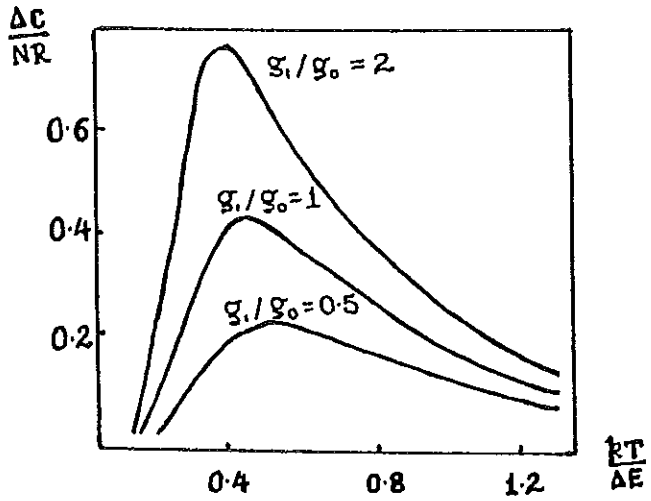

Fig 1.2 contribution of an independent two level system to the heat capacity of a crystal for different values of g_0/g_1

A rapid change in the population of the levels is seen at $kT \sim \Delta E$, and ΔC drops exponentially in the low temperature regions while it drops as the inverse square of T for higher temperature.

There are a number of experimental evidences of heat capacity anomalies of which two of them are presented below.

(i) Spin splitting of the ground state of O_2 molecules.

J.C Burford and G.M Graham [9] reported (1968) that a heat capacity anomally in solidified gases CO and N_2.

The heat capacity of solidified gases CO and N_2, containing O_2 impurities was measured and it is foud that the heat capacity deviate much from the expected T^3 variation. Rotational effects of the impurities or molecules of the solid are not the cause since the crystal field is strong enough to allow only small angular oscillations in both solids , more over both N_2 and CO as hosts display the same anomally (see fig. 1.3).

The explanation to this phenomena lies in the fact that O_2 molecules have uncompensated electron spin s=1. The ground state $^3\Sigma_g^-$ of the electrons split due to the spin-axis interaction. The EPR spectrum shows that for free molecule the separation of the splitted levels is 5.71k which practically coinicide with the value of ΔE=5.14k obtained from heat capacity data. The existance of this two level system in the oxygen impurity is responsible for the observed heat capacity anomally.

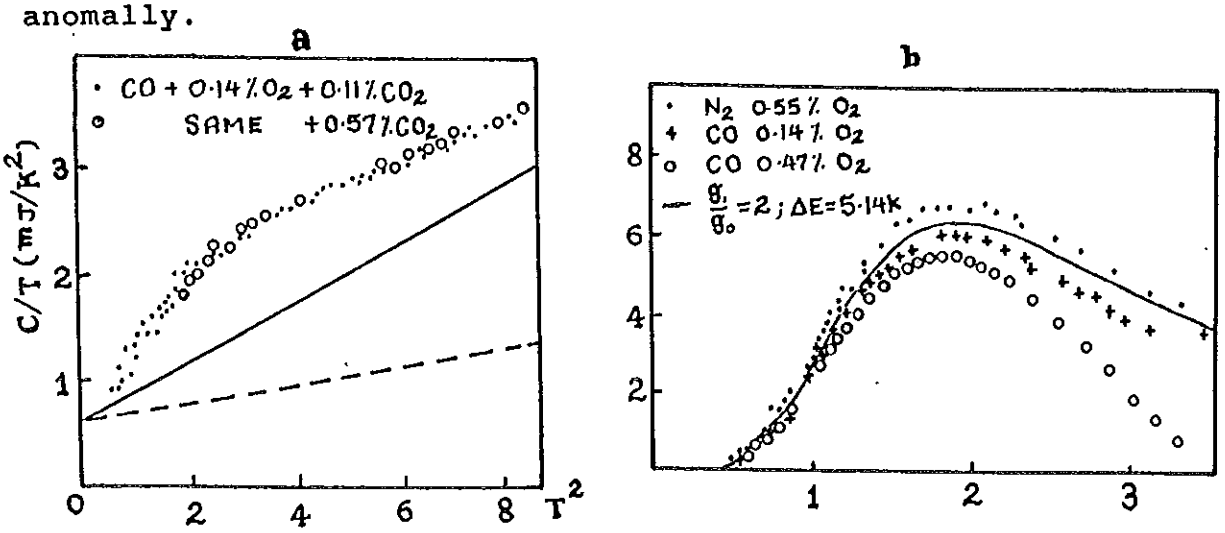

fig 1.3 (a) heat capacity of CO sample with molecular impurities - - - - - empty calorimeter contribution ——— the expected T^3 variation, (b) ——— calculated excess heat capacity for two level system: ΔE=5.14k.

(ii) Nuclear spin species conversion in solid methane

In the solid phase methane has strange property: three-fourth of the molecules in a given sample are strongly oriented in a cog-wheel manner so that only small angular oscillations (called libration) are possible. The remaining one-fourth molecules are nearly freely rotating with in their own lattice. In addition to this methane molecules are found in three spin modifications.

The energy level scheme for ordered (D_{2d} symmetry) molecules indicate that the first excited states are found about 70k above the ground librational states. The excitation to these levels is extremely unlikely at low temperatures. But the ground levels corresponding to each spin species did not lie on the same line in the spectrum. That is conversion between the different spin species amounts transition between the ground levels.

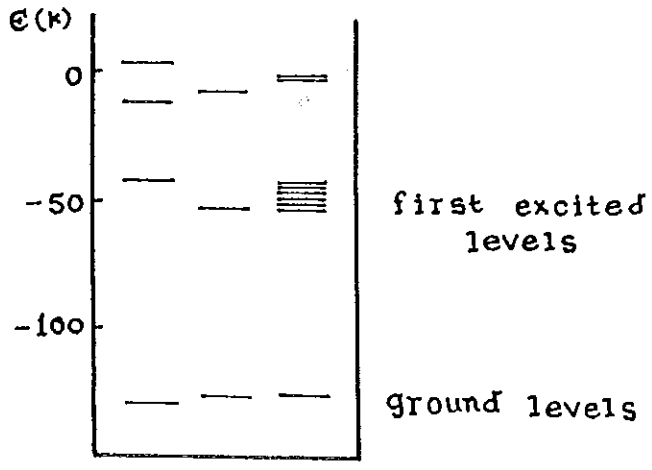

Fig.1.4 Energy level scheme for ordered molecules of methane

Vogt and Pitzer [4], reported low temperature heat capacity studies of methane. An anomaly is observed in the region about 1k. This anomally is attributed to the interconversion between the three ground state levels corresponding to each spin species.

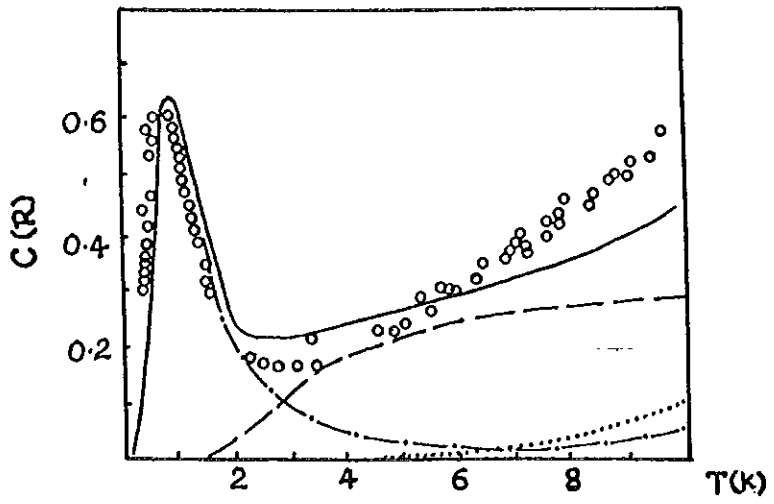

Fig 1-5 Molar heat capacity of solid methane

—.—.—.— contribution from ordered molecules;

— — — — contribution from rotating molecules

..... contribution from lattice specific heat

———— sum of the above three contributions

oooooooo observed values by Vogt and Pitzer

1.2 Investigation of Molecular Spectrum through Heat capacity Analysis

1.2.1 Energy Spectrum of free Diatomic molecules

The internal energy of a diatomic molecule is associated with the internal degrees of freedom of the molecule such as nuclear, electronic, vibrational and rotational. In the case when interaction between them is weak, the total internal energy

of a molecule is given by:

$$\epsilon_{int\epsilon} = \epsilon_{nuc} + \epsilon_{el} + \epsilon_{vib} + \epsilon_{rot} \qquad \ldots(1.6)$$

The energy spectrum of a diatomic molecule and the corresponding temperature is shown below.

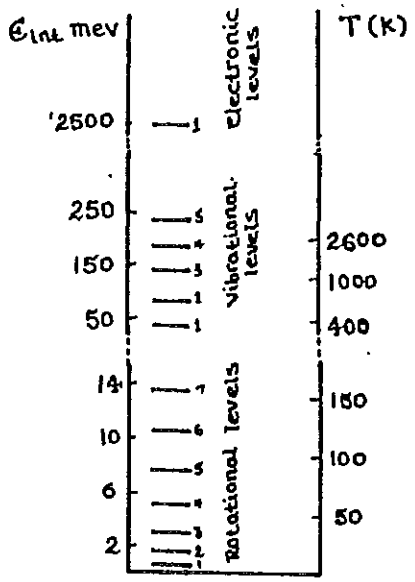

Fig. 1-6 Energy spectrum of a nitrogen molecule.

Fig 1.6 shows that, at very low temperatures the energy associated with the molecules is only rotational. Therefore in the temperature range of our interest (below 12k) we deal only with rotational heat capacity which is mainly due to population and depopulation of rotational levels.

1.2.2 Method of Trapped Molecules in Atomic Matrices

Investigation of the rotational energy spectrum of diatomic molecules is performed by trapping the molecules of interest in

various crystals. When linear molecules are trapped in a crystal, their free rotor spectrum gradually changes to a hindered rotor spectrum and then to the spectrum of angular oscillator (liberator) as the strength of the crystal field hindering the rotation is getting stronger and stronger.

If we consider N_2 molecules in solid nitrogen, the rotation is strongly hindered by the strong crystal field so that only small angular osillations are possible and as a result it is difficult to observe rotational and spin nuclear effects on the heat capacity even at low temperatures. But when nitrogen molecules are trapped in matrices of inert gas crystals, the barrier created by the crystal field of the neighbors and hindering the rotation are much lower. Moreover the rotational characteristic temperature of the molecule are one to two orders of magnitude lower than the Debye characteristic temperature of the crystal matrix. Therefore the rotational heat capacity of the trapped molecules would be observed on the background of the small lattice heat capacity.

Thus this method is cited as the most appropriate to obtain informations on the peculiarites of the rotational spectrum of molecules since impurities introduce an appreciable even sometimes dominant contribution to the thermal properties of week solutions.

1.2.3 Heat Capacity of Solidifyed inert gases with molecular impurities.

The heat capacity of solidifyed inert gases containing molecular impurities is found to exceed the combined heat capacities of the components [1,2]. The excess heat capacity is shown in fig.1-7 below.

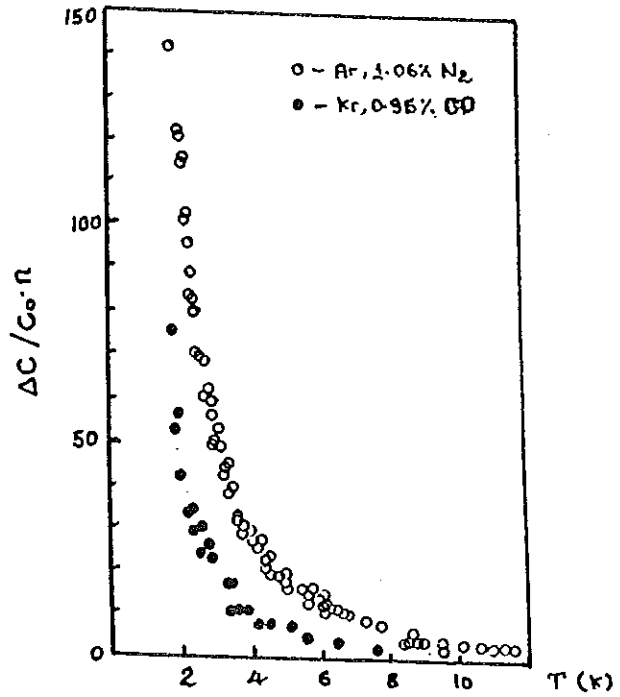

Fig.1.7 relative excess heat capacity of solid solutions

It can be seen from fig 1.7 that the contribution per impurity is from 40 to 150 times larger than the host atom contribution. The heat capacity in excess of the contribution of the components is the attribute of the rotational degree of freedom of the impurity molecules.

The rotational energy spectrum of the molecules, which is responsible for such a large contribution to the heat capacity of the mixture, can be investigated in detail by the heat capacity method as the rotational heat capacity is very sensitive to the detailed features of the energy spectrum.

The total heat capacity of an inert gas matrix containing molecular impurities, thus can be written as

$$C = C_o + \Delta C = C_o + \Delta C_{rot} + \Delta C_{mass} \qquad \ldots(1.8)$$

where C_o is the heat capacity of the pure matrix, ΔC_{rot} is the rotational heat capacity of impurity molecules, and ΔC_{mass} is the contribution to the heat capacity of the solution associated with the difference in masses and force constants of the components of the solid solution.

In calculating ΔC_{mass} it is necessary to take in to

$$\frac{\Delta\Theta}{\Theta_{cry}} = -\Gamma_{cry}\frac{\Delta V}{V_{cry}} = -n\Gamma_{cry}\frac{V_{imp}-V_{atom}}{V_{atom}} \qquad \ldots(1.9)$$

account the change in the Debye temperature of the solid solution $\Delta\Theta$, associated with with the change in volume accompanying the introduction of the impurity is given by eq. 1.9, where

Γ_{cry} , n, V_{imp} and V_{atom} are the Gruneissen constant of the host crystal, number of impurities, volume per impurity and volume of one atom of the host lattice respectively.

By definition $\Gamma = d\ln\Theta/d\ln V$, and experiment shows that $\Gamma = \beta V/\Delta C_m \chi_T$, where β and χ_T are coefficient of volume expansion and isothermal compressibility. From these two relations we obtain for ΔC_m as

$$\Delta C_m = [\beta V/\chi_T]\,[d\ln V/d\ln\theta] \qquad \ldots(1.10)$$

The experimentally determined quantity is C, if we know C_o, the heat capacity associated with the impurities is thus

$$\Delta C = \Delta C_{rot} + \Delta C_m = C - C_o$$

therefore

$$\Delta C_{rot} = C - C_o - \Delta C_m \qquad \ldots(1.11)$$

The value of C_o is experimentally determined by Finegold, Morrison etal. [10], and Manzhelli etal. [2]. All the results agree except of small discrepancies within the limit of the experimental error. The results are compared in fig. 1.8.

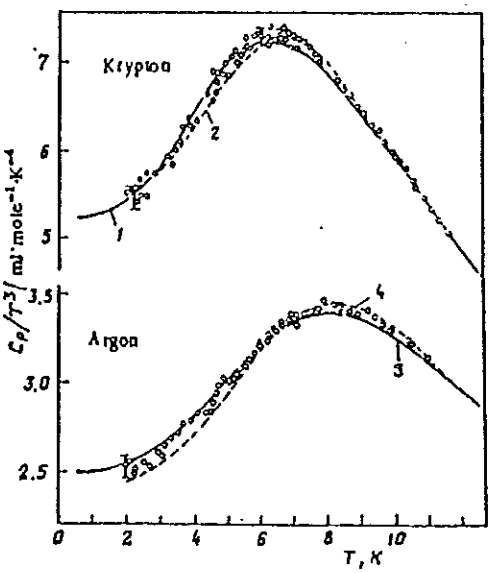

Fig 1-8 Heat capacity of high purity krypton and Argon. o) experimental points from the work of Hanrhelliital. curves 1) Fine gold 2) Beaumont, ohihara and Morrison 3) Finegold, 4) Flubacher, Leadbetter, and Morrison [2],

CHAPTER II ROTATIONAL HEAT CAPACITY OF DIATOMIC MOLECULES : THEORETICAL MODELS

The rotational energy spectrum of linear molecules must be known for correct theoretical computation of the heat capacity associated with this degree of freedom. The question of how the rotational states and hence the energy spectra of free molecules were modified when they crystallize into a lattice arose in 1930 and led to the develpoment of different theoretical models. No single model capable of describing all experimental facts is developed to this day. In the first section of this chapter the free rotational heat capacity of linear molecules is computed in order to estimate the temperature region in which the rotational heat capacity is important and to adapt the methods of calculation for hindered rotor heat capacity. In the last two sections two theoretical models describing the rotational spectrum of linear molecules are reviewed.

2.1 Free Rotor Heat Capacity

In the case when the impurities are considered free in the crystal the total internal energy (U_{int}) of the solution can be considered as the sum of the internal energy associated with the lattice (E_{lat}) and the rotational energy associated with the

impurity (E_{rot}). Thus for n impurities and average energy per impurity $\langle\epsilon\rangle$ we have $E_{rot} = n\langle\epsilon\rangle$ i.e.

$$E_{rot} = n\left[\frac{\sum_j g_j \epsilon_j \exp(-\epsilon_j/kT)}{\sum_j g_j \exp(-\epsilon_j/kT)}\right]$$

...(2.1)

The contribution of the rotational energy to the heat capacity is thus:

$$\Delta C_{rot} = \frac{\partial E_{rot}}{\partial T} = \frac{n}{kT^2}\left[\frac{\sum_j g_j \epsilon_j^2 \exp(-\epsilon_j/kT)}{\sum_j g_j \exp(-\epsilon_j/kT)} - \left(\frac{\sum_j g_j \epsilon_j \exp(-\epsilon_j/kT)}{\sum g_j \exp(-\epsilon/kT)}\right)^2\right]$$

...(2.2a)

i.e

$$\Delta C_{rot} = \frac{n}{kT^2}\left[\langle\epsilon^2\rangle - \langle\epsilon\rangle^2\right]$$

...(2.2b)

g_j and ϵ_j are the degeneracy and the energy associated with the j^{th} rotational level.

Now equation 2.2a is equated for all values of the rotational quantum numbers j. But we are dealing with the case of homonuclear diatomic molecules, in which exchange of the two identical nuclei can not be accepted as a possible operation leading to a new state of the molecule according to quantum statistics. This restriction imposes a requirement on the

symmetry of the wave function describing the possible states of the molecule and gives rise to a relation between the rotational wave function and nuclear spin wave function.

Therefore the rotational partition of a homonuclear diatomic molecule is viewed as the sum of symmetric and antisymmetric rotational wave functions represented respectively as

$$Z_{rot}=\sum_{j=0,2,4,\ldots} g_j \exp(\epsilon_j/kT)+\sum_{j=1,3,5\ldots} g_j \exp(\epsilon_j/kT) \qquad \ldots(2.3a)$$

$$\text{i.e}\quad Z_{rot} = Z_{even} + Z_{odd} \qquad \ldots(2.3b)$$

And the nuclear partition function is just the number of spin states :

$$Z_{nuc} = (S+1)\ (2S+1)\ , \text{ symmetric spin states} \qquad \ldots(2.4a)$$

$$= S(S+1)\ , \text{ antisymmetric spin states} \qquad \ldots(2.4b)$$

Now two cases arise :

(i) nucleus Bose particle (the total wave function Φ of the molecule must be symmetric), therefore

$$Z_{nuc-rot} = (S+1)(2S+1)\ Z_{even} + S(2S+1)\ Z_{odd} \qquad \ldots(2.5a)$$

(ii) nucleus Fermi particle , Φ must be antisymmetric so that

$$Z_{nuc-rot} = S(2S+1)\ Z_{even} + (S+1)(2S+1)\ Z_{odd} \qquad \ldots(2.5b)$$

In the high-temperature limit the sum over the even levels and odd levels are equal, showing that the composition

ortho:para is constant at high temperatures. In the case of nitrogen the high temperature composition is retained even down to 2k [2], which gives an opportinuity of computing the heat capacity contribution of different spin species separately:

$$\Delta C_{rot} = \Delta C_g + \Delta C_u \qquad \ldots(2.6)$$

where ΔC_g is the rotational heat capacity contribution of the molecules characterized by symmetric wave functions, while ΔC_u is of those characterized by antisymmetric wave functions. ΔC_g is obtained from equation 2.2a for even j values and so is ΔC_u for odd j values in equation 2.2a.

The high temperature distribution of the spin nuclear modifications of $^{14}N_2$ and $^{15}N_2$ is in such a way that 2/3 of $^{14}N_2$ (ortho-$^{14}N_2$) or 1/4 of $^{15}N_2$ (para-$^{15}N_2$) molecules occupy the rotational levels characterized by symmetric wave functions and 1/3 of $^{14}N_2$ molecules (para-$^{14}N_2$) or 3/4 of $^{15}N_2$ molecules (ortho-$^{15}N_2$) occupy levels of antisymmetric wave functions. Hence impurity component of heat capacity can be presented in the form:

$$\Delta C_{rot} = \frac{2}{3}\Delta C_g + \frac{1}{3}\Delta C_u$$

nitrogen-14 ...(2.7a)

and

$$\Delta C_{rot} = \frac{1}{4}\Delta C_g + \frac{3}{4}\Delta C_u$$

nitrogen-15 ...(2.7b)

For free rotation $g_j = j(j+1)$, $\epsilon_j = j(j+1)B$; and using the rotational characteristic temperature $\theta_{rot} = B/k = 2.7581$ kelvin for $^{14}N_2$, in equation 2.2a and equation 2.7a the temperature dependence of the free rotational heat capacity of $^{14}N_2$ is shown in fig. 2.1 below.

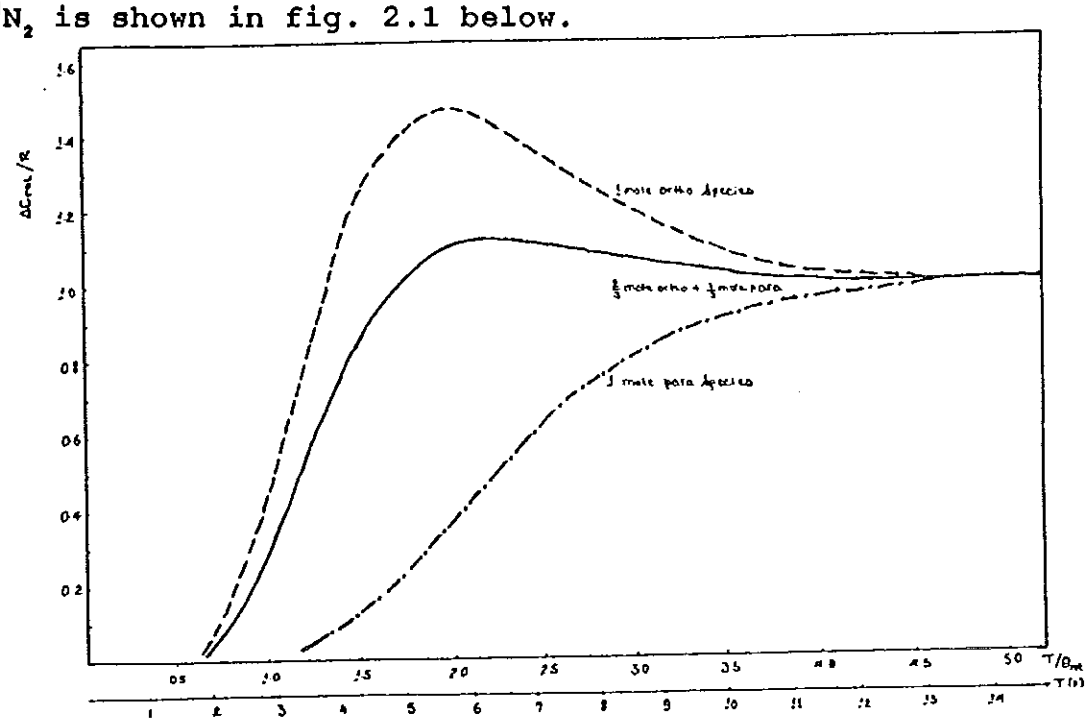

Fig 2.1 Free rotational heat capacity of $^{14}N_2$: — — — one mole of pure ortho, —·—·— one mole of pure para, ——— 2/3 Δ C_g + 1/3 Δ C_u

It is evident from fig 2.1 that significant spin nuclear and rotator effects appear below 12k. For higher temperatures the rotational heat capacity of both modifications converge to their classical value: $C_{rot}=R$, for one mole.

2.2 Hindereed Rotor Heat capacity

2.2.1 Devonshire Model

One of the first theoretical models developed for describing hindered rotation was Devonshire's model.

A.F. Devonshire [5], calculated the effect of a crystalline field of octahedral symmetry on the rotational states of a linear molecule. For this he chose a potential of the form

$$V(\theta,\phi)=\frac{-K}{8}[3-30\cos^2\theta+35\cos^4\theta+5\sin^4\theta\cos 4\phi] \quad \ldots(2.8)$$

where θ and ϕ are polar coordinates and K is the potential parameter associated with the height of the barrier.

The Devonshire potential has six maxima, equal to -K along the six <100> directions of a cube, eight maxima equal to 2K/3 along the <111> direction for K>0. Such a potential is used if the molecule has equilibrium orientiations along the <100>

directions.

For K<0, the maxima and minima of the above case are interchanged and this kind of potential is used if the molecule has equilibrium orientiations along the <111> directions.

For all K, V has saddle points in the twelve <110> directions.

In using the Devonshire's potential the tacit assumptions made are: (i) the nieghboring atoms of the impurity molecules are stationary, (ii) the potential has full octahedral symmetry undistorted by random stresses or by the impurity itself, and (iii) the motion of the impurity can be considered as a purely rotational one described by the two spherical coordinates θ and ϕ alone.

Based on the above assumptions the eigenvalues of the Schrodinger equation for a molecule of rotational constant B, were computed by Devonshire and also recently by Sauer [12], as a function of the potential parameter K.

The spectrum of eigen values in units of B obtained by Devonshire is shown in fig 2.2. For K=0, the energy levels are of a free rotator and j(j+1) fold degenerate for the j^{th} level. With large |K|,the energies in fig 2.10 change from those of a free rotator to those of a librator librating in six or eight wells for positive and negative values of K respectively.

For intermediate values of |K|, however the degenerate levels of the free rotor split under the influence of the octahedral symmetric field of the crystal.

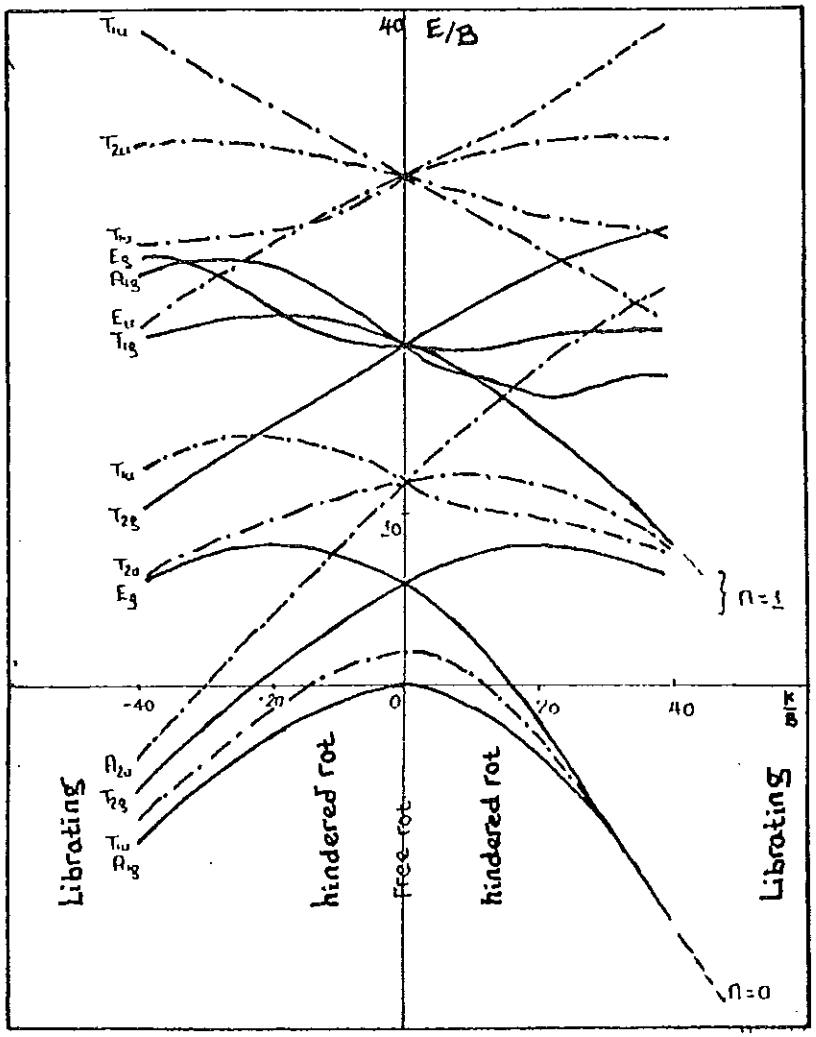

Fig. 2.2 The Rotational states of a linear rotator in the Devonshire potential.

The split of the levels is according to table 2-1 shown below. The labeling of the energy levels corresponds to the irreducible representation of the octahedral symmetry group.

J		J	
0	A_{1g}	1	T_{1u}
2	$E_g + T_{2g}$	3	$A_{2u} + T_{1u} + T_{2u}$
4	$A_{1g} + E_g + T_{1g} + T_{2g}$	5	$E_u + 2T_{1u} + T_{2u}$

etc

Table 2-1 splitting of rotational energy levels in a field of octahedral symmetry.

As is true in any spectrum of energy levels, in computing rotational heat capacity of hindered rotor by using Devonshire spectrum, what matters is not the actual energy value of a given level , but the elivation of the level from the ground level. In our case the A_{1g} level the ground level for molecules described by symmetric wave functions while the T_{1u} level is for molecules described by antisymmetric wave functions. The spectrum of a linear rotator in Devonshire potential as measured from the A_{1g} level is plotted in fig 2.3.

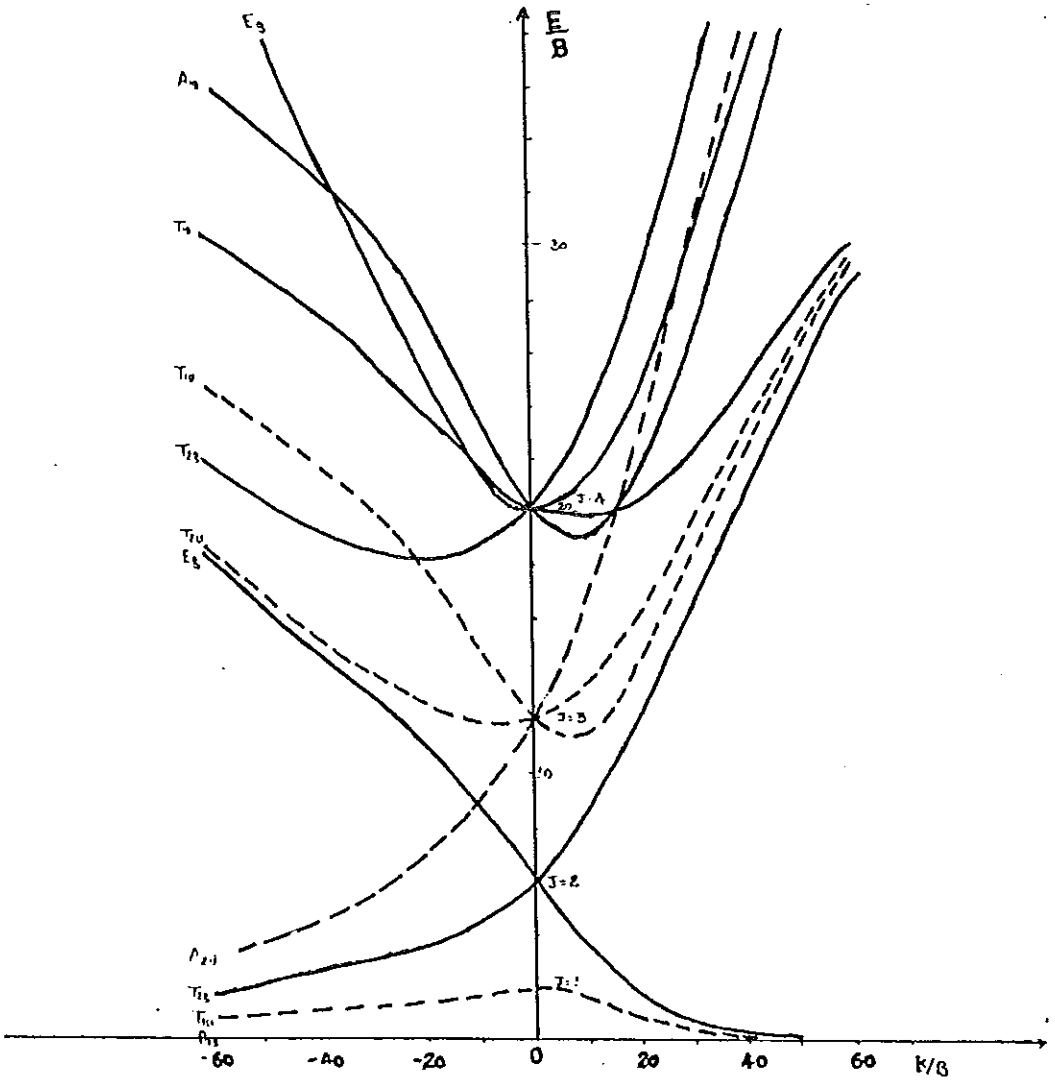

Fig 2.3 The spectrum of a linear rotator in Devonshire potential as measured from the A_{1g} level.

———)even values of J, — — —)even values of J.

The rotational heat capacity of diatomic molecules, in the Devonshire model, is computed theoretically by the use of this spectrum, in equation 2.2a. It should be noted at this point that for homomuclear diatomic molecules, each level corresponding to antisymmetric wave function must be measured from the T_{1u} level before we use the energy values in equation 2.2a for odd j.

2.2.2 Manz -Mirsky Model.

Devonshire's model and its generalizations has been widely used for interpreting different types of experiments [3], as will be shown in section 2.3, failures are observed in the interpretation of calorimetric data based on Devonshire's model.

Suspecting its neglect of the relaxation of the environment of impurity molecule as the most significant deficiency of Devonshire's model, J.Manz [6] and K.Mirsky [7] developed a model of rotating molecule in a crystal matrix.

According to Manz and Mirsky, the non-sphericity of the molecule gives rise to anisotropy of the impurity-lattice interaction and leads to anisotropic lattice relaxation. The cage's shape and its alignment thus resemble that of the molecule. Thus as the molecule turns the cage appears to rotate with the molecule, provided that lattice relaxations are faster than the rotation of the molecule so that the molecule always find itself in a synchronously rotating cage. The rotation of the cage is referred to as pseudorotation for the constituent atoms of the cage are actually oscillate about their undistorted lattice site cooperatively. (see fig 2.4).

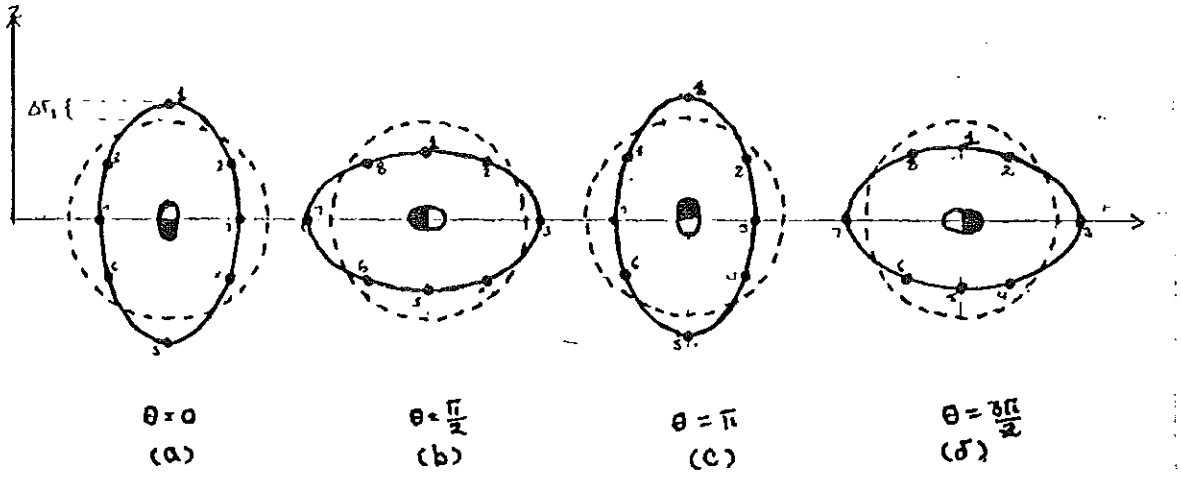

Fig 2.4 Rotating linear molecule in synchronously pseudorotating cage (schematic). The molecule is shown as a black-white ellipsoid together its nearest neighbors (black dots) in four successive phases. (a), (b), (c), and (d) show instantaneous equilibrium positions linear molecule rotating in the Y-Z plane, for different values of θ

As the result of such synchronous rotation of the molecule and psudorotation of the relaxation region two important effects, that lead to renormalization of the Devonshire model parameters, viz the potential parameter K of the crystal field and the rotational constant B of the impurity molecule, will occur.

The first one is an increase of the effective moment of inertia of the guest molecule induced by the orientation dependent lattice relaxations, which is given by:

$$I_{eff} = I_o + \Delta I_1 + \Delta I_2 \qquad \ldots(2.9)$$

where I_o is the gas phase moment of inertia of the guest molecule, ΔI_2 is the contribution due to the effective rotation of the center of mass of the mollecule around the center of interaction, and ΔI_2 is the contribution of the pseudorotating cage.

For homonuclear diatomic molecules, the center of mass and center of interaction coinicide. Therefore in our case the second term in equation 2.9 is zero. In the theory of Manz and Mirsky, ΔI_2 is estimated from the kinetic energy of the oscillating atoms on the pseudorotating cage, and it is shown to be

$$\Delta I_2 = 2 \sum_i m_i \Delta r_i^2 \qquad \ldots(2.10a)$$

The new effective moment of inertia is thus

$$B_{eff} = \frac{h^2}{8\pi^2 I_{eff}} = B(I/I_o)$$

$\ldots(2.10b)$

The second effect of the non-rigidity of the lattice and synchronous rotation of the cage is that the decrease in the

molecule-crystal interaction energy for a given orentation of the impurity. In the theory Manz and Mirsky, approximated the total interaction potential energy assuming it retains its global minimum as the sum of the intramolecular potential, (V_m), the interaction potential of the matrix and the molecule.

In Devonshire's model, the impurity "sees" octahedral symmetry due to the geometry of the rigid lattice. But in this model the instantaneous geometry around the impurity has lower octahedral symmetry having equivalent lattice distortions led by equivalent reorientations so that the symmetry is retained. Hence the Devonshire spectrum could be used for the renormalized values of K and B. Since Manz-Mirsky model, finally counts on the Devonshire spectrum for renormalized B and K, it is reffered to as the Devonshire-Manz-Mirsky (DMM) model.

In computing theoretical heat capacity with in the framework of the DMM model the renormalized K and B are adjusted so as to obtain a good fit with experiment, for the theoretical evaluation of these parameters is still approximate.

2.3 Review Of Experimental Results.

The recent experimental investagations of the heat capacity of linear diatomic molecules available in literatuer are those of Manzehelli et al [2], and Sumarkov etal [1], 1986 and 1984 respectively. In these papers the specific heat and thermal expansion of solutions of $^{14}N_2$, $^{15}N_2$ and CO in solid Ar and Krhave been studied in the temperature range 2 to 12k with the aim of investigating the rotational motion of linear impurity molecules.

Some of the systems investigated and the conclusions drawn are presented here to help for comparison in latter sections:

(i) Kr-CO, 0.95mole%CO.

(ii) Ar-$^{14}N_2$, 1.06 mole% $^{14}N_2$

(iii) Kr-$^{14}N_2$, 0.95 mole% $^{14}N_2$

(iv) Kr-$^{15}N_2$, 1.02 mole%$^{15}N_2$

(v) Ar-$^{15}N_2$, 1.08 mole%$^{15}N_2$

The lattice parameters and the interatomic distance of the molecules (in angstrom units); with the rotational constant (in kelvin) of the molecules, is given in table 2.2.

	Kr	Ar	$^{14}N_2$	$^{15}N_2$	CO
R(Å)	3.9922	3.7555	3.994	3.989	3.992
B(k)			2.8751	2.6840	2.7787

Table 2.2 lattice parameters and interatomic distances.

Table 2.2 shows that the molar volume of the impurity exceeds that of the host lattice in systems (ii) and (v). In the theoretical computation of the rotational heat capacity it is therefore necessary to take in to accout the change in Debye tempartures for these systems.

In all cases the specific heat of pure solid Kr and Ar was measured and found to agree with earlier results [10], the extracted impurity heat capacity of the above systems is briefly discussed in what follows.

(i) Kr-CO, 0.95 mole%CO, fig 2.5

The experimental values of the excess heat specific heat ŠC, of the Kr-CO solution with CO concentrtation of 0.95mole% are shown in fig 2.5

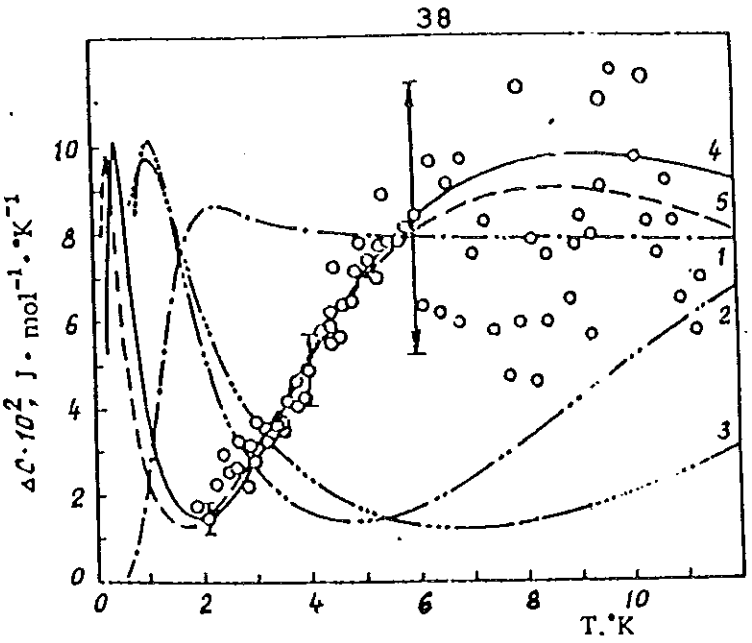

Fig 2.5 Excess specific heat Δ C of a Kr-CO solid solution .Experment.) experimental points, Theory: curve 1) free rotor, 2)Devonshire's model K=20, 3)Devonshire model K=-60, 4) DMM model K=20; B=1.11, 5) DMM model K=-60; B=0.69.

The results of calculations predicted on the basis of Devonshire model (curves 2 and 3) and on the assumption of freely rotating impurity molecule (curve 1) fail to explain the experimental results for all K even qualitatively. At the same time the experimental results can be fairly well described with in the frame work of the DMM model. Agreement between experimental points and the computed curve is obtained for K =20 and K=-60 (curves 4 and 5 respectively). As can be seen from fig 2.5 the choice between positive and negative values of K remain umbiguous unless the measurements are extended below 2k where the two curves differ markedly.

The experimental results scatter above 6k this is due to the fact that the background lattice vibrational heat capacity

is increasingly dominant contributor to the total heat capacity of the solutions with temperature and extraction of the impurity component of the heat capacity will be increasingly uncertain.

The vertical double arrows on this figure and in the coming sections indicate the overall error in extracting the impurity component of the heat capacity.

$^{14}N_2$ in Ar and Kr

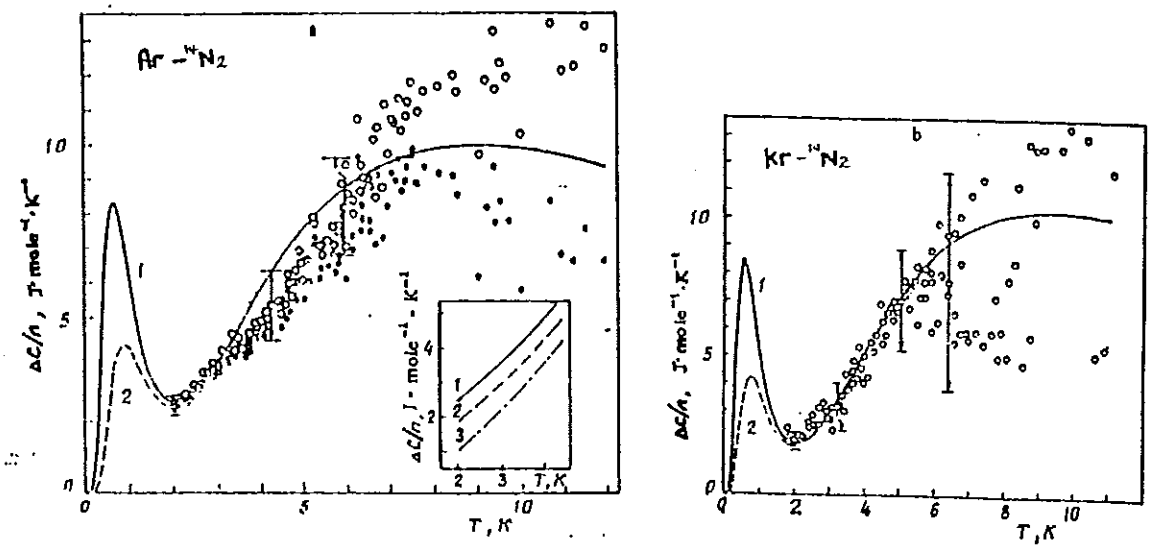

Fig. 2-6, Excess heat capacity due to rotation of $^{14}N_2$ in Ar and Kr, (a) 1.06 mole% N14 inAr, (b) 0.95 mole% N14 in Kr.

(ii) Ar-N14, 1.06mole% N14 fig 2.6a

Experiment o)neglecting the change in the Debye temperature; •) taking in to account the change in the Debye temperature.

Calculation: a good agreement is obtined on the framework of DMM model, for K=18 and B=1.15. curves: 1) assuming conversion between ortho- and para- species. 2) assuming the

high temperature composition is frozen.

The two curves practically coincide above 2k, but differ significantly in the low temperature region both in magnitude and in the positions of the low temperature peak (0.6k for equilibrium and ~ 0.85k for the hightemperature composition).

The figure also shows that the correct hightemperature assymptotic behavior of Δ C is obtained when the change in Debye temperature due to the inserttion of nitrogen molecule, having greater molar volume in Ar, is taken in to account.

Curves 1,2,and 3 in the inset of fig 2.6a show the curve Δ C/n for 1.06, 1.87 and 5 mole% $^{14}N_2$ respectivelly. There is a significant concentration nonlinearity, consisting at 3k of 25% for 2mole% and 50% for 5mole% $^{14}N_2$. Since the direct interaction of the impurity molecules is weak, the observed nonlinearity is apparently associated with the dynamic interaction of the regions of relaxation, surrounding each impurity molecule.

(iii) Kr-N14, 0.95 mole%N14 fig 2.6b

Experiment o) experimental points.

calculation DMM model agreement with the experimental points is obtained for K/B=20; B=1.15.

It is evident from table 2.2, the molar volumes of Kr and $^{14}N_2$ are practically the same. There is no need to account for the change in Debye temperature and itis natural to expect that the rotation of nitrogen molecules in Kr is close to free rotation than in Ar, but analysis of expreimental result shows the contrary (see fig 2.6b).

$^{15}N_2$ in Kr and Ar

The other isotope of nitrogen is also studied in Ar and Kr so as to investigate the influence of the nuclear spin on the rotational heat capacity. It is worth remembering that the nuclei constituting $^{15}N_2$ are Fermi particles while those of $^{14}N_2$ are Bose particles.

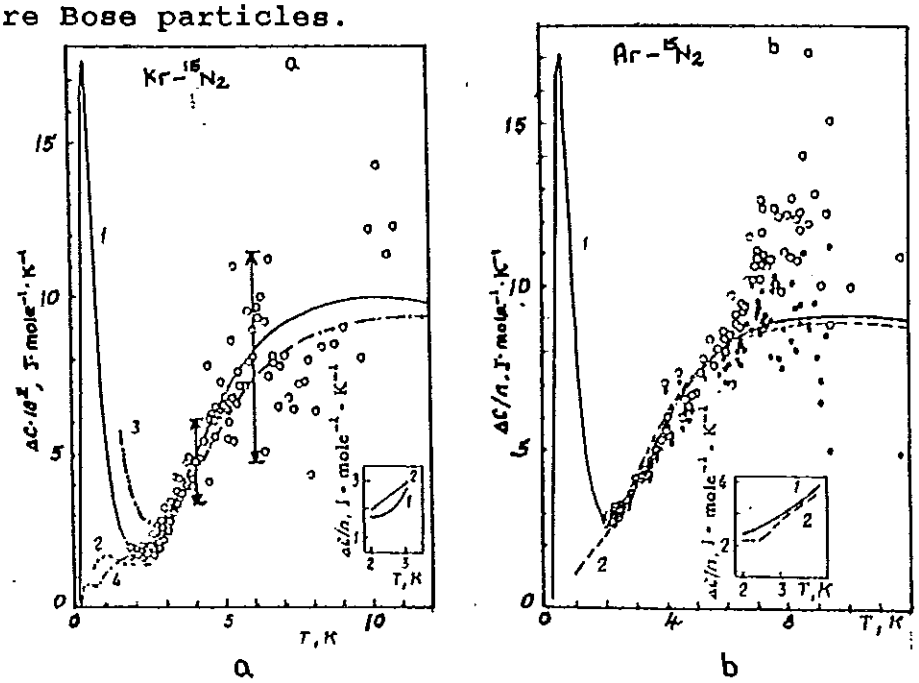

Fig 2.7 Excess heat capacity due to rotation of $^{15}N_2$ in Kr and Ar. (a) 1.02 mole%N15 in Kr, (b) 1.08 mole%N15 in Ar.

(iv) Kr-$^{15}N_2$, 1.02 mole%N15, fig 2.7a

Experiment o) experimental points.

calculation: DMM model and taking in to account the the contribution of $^{14}N^{15}N$ and $^{14}N_2$ to the heat capacity of $^{15}N_2$. A good agreement between the calculation and the experimental points is achieved for K=16 and B=1.34. Curves: 1) equilibrium; 2) high temperature distribution of the nuclear spin modifications. Curves 3 and 4 in the figure are drawn for K=13; B=1.80. This shows the parameters B and K can not be determined uniquely based on high temperature measurements only.

The difference between the the equilibrium and frozen high temperature curves the the case of $^{15}N_2$ are sharper than in the case of $^{14}N_2$ (cf. fig 2.5a and b), which makes the $^{15}N_2$ impurity more promising for the solution of the problem of conversion in nitrogen.

The peak in curve 4 is determined by the contribution of a small amount of $N^{14}N^{15}$ (7% of the total impurity molecules) to the Δ C. The inset in the fig shows the smoothed experimental

curves Δ C/n, for nitrogen in Kr:1) 1.02, 2) 0.95 mole% $^{15}N_2$.

(v) Ar-$^{15}N_2$, 1.08mole%$^{15}N_2$, fig 2.7b.

Experiment: o) neglecting the change in the Debye temperature.

•) taking in to account the change in the Debye temperature.

Calcualation: DMM model: the agreement between the computed curves and experimental result is obtained for K=13, B=1.34 and also for K=10; B=1.51. Curve 1, is for equilibrium distribution and 2 is for frozen hightemperature distrbution.

The inset shows Δ C/n for concentrations 1) 1.08 mole%; 2)1.90 mole%.

To sum up what we have in literature, in the DMM model the shift in the matrix atoms that is produced by rotation of impurity molecules is effectively taken in to account by reducing rotational constant of the molecules and by renormalization of the parameter K of the crystalline field which hinders the rotation. Thus, the effective rotational constant of an impurity molecule is two to three times smaller than the rotational constant of a free molecule B for all systems that have been studied. The corresponding rotational motion of an impurity molecule is compressed 2 to 3 fold compared with the spectrum of molecule in a rigid matrix. With appropriate selection of K and B the DMM model provides a fairly well explanation for observations in the temperature region above 2k.

The next step in the study should thus be the extension of the measurements in to the temperature region below 2k. It is the theme of this work to analize experimental data below 2k.

CHAPTER III LOW TEMPERATURE HEAT CAPACITY DATA $^{14}N_2$ AND $^{15}N_2$ IN Ar AND Kr

3.1. THE EXPERIMENT

Recent experimental data of the impurity component of the heat capacity of Ar-$^{14}N_2$ solid solutions with nitrogen concentrations n=0.12, 0.25, 0.5, 1.02, and 2.74 mole%; Ar-$^{15}N_2$ solid solutions with nitrogen concentrations, n=0.13 and 0.24 mole%, and Kr-$^{14}N_2$ solid solutions with nitrogen concentrations 0.13, and 0.24 mole% is obtained from physicotechnical institute of low temperatures Acadamy of scienses of the Ukrainian SSR Kharkov and used for the analysis in this work.

For all systems measurements were taken starting from 0.5k in order to include temperature regions where the heat capacity of dilute solutions is strongly dominated by the rotational heat capacity of diatomic impurity molecules and excitations of the low lying rotational levels are predominant contributors to the rotational heat capacity of the impurities, with the hope of obtaining new informations.

3.1.1 Experimental methods and Apparatus.

The study of the specific heats of cryocrystals and their mixtures is done in an adiabatic calorimeter usually capable of

studies over temperature range 0.4-300k.

For T<2k experimental difficulties arise due to the low specific heat of the material, the increase in the relative contribution of the heat capacity of the calorimeter, the increase in the kapitza resistance between the elements of the calorimetric cell (thermocouples, thermometers, heaters, walls of the calorimeter and the sample), and the increased requirements for stability of the temperature transducers and the precision of their calibration. The influences on the measurement precisoion due to vibrations, electrical induction, parasitic emfs, power dissipation in the thermometers, etc are significant.

In the design and preparation of a calorimeter, one has to attempt as much as possible to reduce the influence of these factors on the measurement precision. The techniques and experimental methods used to obtain the data analized in this work are briefly described in this subsection.

(i) Cryostat and Calorimetric cell.

Schematic drawing of the cryostat is shown in fig 3.1 below.

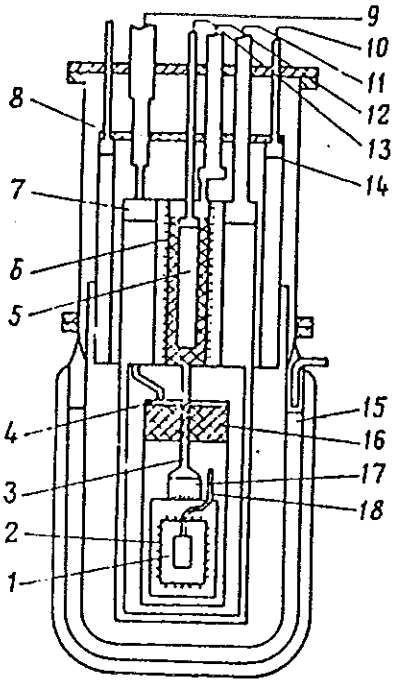

Fig 3.1 Schematic drawing of the cryostat: 1) calorimetric cell; 2) adiabatic screen; 3, 9, 10, 11, 12, 13) tubes; 4) diaphragm; 5) helium chamber of the adsorption pump; 6) heater for the adsorption pump; 7) auxiliary helium chamber; 8) detachable vacuum chamber; 14, 15) nitrogen chamber; 16) working chamber with ^4He; 17) chamber with ^3He; and 18) capillary fill tube.

The major parts of the cryostat are the detachable vacuum chambers, the nitrogen baths 15 and 14, the auxiliary helium bath 7 (T=4.2k), the working helium chamber 16 (T ~ 1.2k), the chamber 17 containing ^3He, the adsorption pump and the calorimetric cell.

The calorimetric cell in the crystat is constructed to enable to create a significant temperature gradient along the steel portion of the calorimetric vessel, which is necessary for the preparation of a homogenous solid solution. The details of the calorimetric cell is shown in fig. 3.2.

(ii) Preparation of Samples.

In the study of mixtrures it is very important to obtain

samples homogenous with respect to concentration. The elements of the calorimeter which made it possible to produce homogenous solid solutions (from the gas phase, by passing the liquid) are shown in fig. 3.3.

Gaseous mixtures of a given concentrations are prepared at room temperature. Solid solutions that are homogenous in concentration and having a mass of 0.5 to 0.7 moles will be grown in the calorimeter from the gaseous phase at a rate of 2.10^{-5}mole/sec at temperatures of 60-70 k. The masses of the mixtures can be determined from the P-V-T data. The uncertainity in determining the masses of the mixture in the experiments of which we use the data is ± 2% for all the solutions.

(iii) Methods of measurement and mesaurement apparatus.

Methods typical for adiabatic calorimeters were used in the measurement of the specific heat. Heat was introduced by an electric current. The current, the voltage drop across the calorimeter heater and the resistance of the therometers were measured potentiometrically. The adiabaticity of the calorimeter is determined by the magnitude of the heat exchange dQ_{ex}/dt between the calorimeter and the external medium. The size and stability of dQ_{ex}/dt determine the sensitivity of the calorimeter, the measurement precission, the time t_m for individual measurements of the specific heat, the equilibrium temperature (at which the power dissipated in the thermometers

is compensated by the heat exchange) and the temperature drift.

Adiabatic operation was ensured in two ways:by the calorimeter screen combination and by the calorimeter and the "control point" on the fill capillary.

The temperature of the calorimeter vessel is measured by resistance thermometer made of carbon and germanium. The detailed description about the construction of such calorimeters is available in ref. 7.

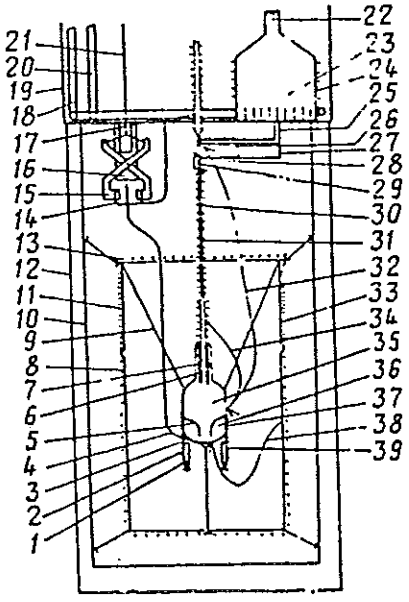

Fig 3.2 Low temperature portion of the cryostat: 1) germanium resistance thermometer; 2, 11) heat exchange conductor; 3) copper shell; 4) calorimeter cooling path; 5) heat exchanger; 6) copper fill capillary; 7) stainless steel tube system; 8) adiabatic screen; 9) silk thread; 10) assembly stand; 12) radiation shield; 13) electric charge; 14) cooling path for the mechanical switch; 15) mechanical heat switch; 16) bracket; 17, 30) heater for fill capillary; 18) input of flow switch; 19) holder; 20) output of flow switch; 21) control rod; 22) filling tube of ^{3}He chamber; 23) ^{3}He chamber; 24) heater for ^{3}He chamber; 25) cooling path with ^{4}He film; 26, 28) heaters for cooling paths; 27) copper cooling path; 29, 39) carbon resistance thermometer; 31) stainless steel fill capillary; 32) thermocouple for calorimeter and fill capillary; 33) heater for adiabatic screen; 34) thermocouple for top and bottom of calorimeter; 35) upper portion of calorimeter chamber; 36) lower portion of calorimeter chamber; 37) calorimeter heater; 38) thermocouple between shield and calorimeter.

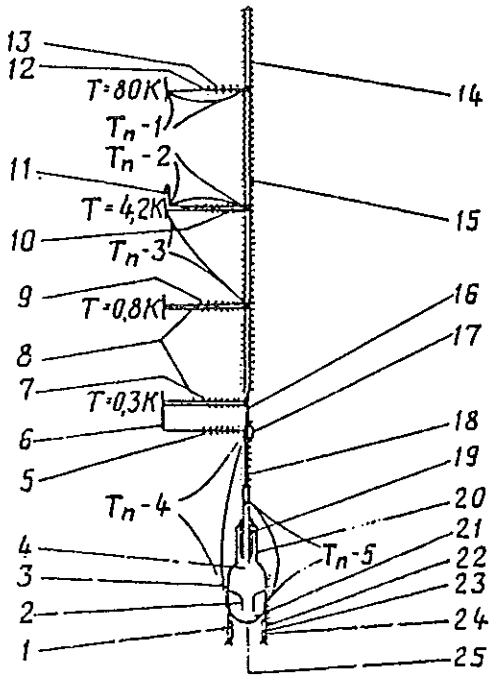

FIG. 3.3 Schematic of the condensation system: 1) germanium resistance thermometer; 2) heat exchanger; 3) calorimeter heater; 4) upper portion of calorimeter vessel; 5, 7, 9, 10, 13) heaters on the cooling paths; 6, 12) copper cooling paths; 8) cooling paths with ^{4}He films; 11) controlled cooling path; 14) stainless steel film capillary (diameter 2× 0.12 × 2000 mm); 15, 18) heaters on the fill capillary; 16) stainless steel fill capillary (diameter 1.6× 0.12× 150 mm); 17, 23) carbon resistance thermometer; 19) copper fill capillary (diameter 2× 0.2× 85 mm); 20) stainless steel tube system; 21) lower portion of the calorimeter vessel; 22) copper shell; 24) heat exchange path; 25) cooling path for the calorimeter; Tn1, 2, and 3 are copper–constantan thermocouples; Tn4 and 5 are Cu–Au + 0.07% Fe thermocouples.

3.1.2 Experimental Results.

The specific heat of pure Ar and Kr was measured in the temperature range 0.5-12k in the same calorimeter to elliminate systematic errors.

The specific heat ΔC, due to the rotational degrees of freedom of N_2, was obtained by subtracting the lattice component from experimentally determined specific heat of the solution. The changes in the specific heat of the lattice associated with the different masses and force constants, for concerned cases, were not taken in to account since this corrections are less than the experimental errors of measurement for concentrations n<1%.

The measured values of $\frac{\Delta C}{n}$ for the systems studied are tabulated below.

T(k)	.12mol%	.25mol%	.50mol%	1.02mol%	2.74mol%
.5	0.	1.728	1.316	0.671	0.347
.6	2.292	2.344	1.824	1.078	0.533
.7	2.967	2.932	2.340	1.265	0.730
.8	3.392	3.404	2.700	1.480	0.847
.9	3.808	3.804	3.000	1.706	1.018
1	3.942	4.000	3.160	1.912	1.215
1.2	4.175	4.240	3.440	2.186	1.401
1.4	4.125	4.240	3.580	2.402	1.667
1.6	4.083	4.040	3.560	2.745	1.894
1.8	4.000	3.960	3.560	2.696	2.142
2	3.808	3.864	3.560	2.892	2.383
2.2	3.675	3.820	3.560	3.098	2.605
2.4	3.633	3.776	3.580	3.324	2.891
2.6		3.720	3.600	3.480	3.146
2.8		3.820	3.760	3.775	3.405
3		3.908	4.060	4.010	3.686
3.5		4.360	4.900	4.696	4.526
4		5.160	5.600	5.451	5.365
4.5		5.840	6.320	6.333	6.313
5		6.560	7.100	7.578	7.153
5.5					7.883
6					8.649
7					9.598
8					10.656
9					11.423
10					12.080
11					12.226

Table 3.1 Ar-$^{14}N_2$ solid solutions with diferent concentrations: Impurity component of heat capacity (Joules/mole kelvin)

T(k)	0.13mole%	0.24mole%
.5	2.462	2.700
.6	2.915	3.021
.7	3.223	3.358
.8	3.362	3.475
.9	3.323	3.450
1	3.231	3.350
1.2	2.969	3.146
1.4	2.715	2.921
1.6	2.415	2.683
1.8	2.131	2.463
2	2.038	2.363
2.2	2.015	2.363
2.4	2.015	2.446
2.6	2.038	2.558
2.8	2.092	2.733
3		2.938
3.5		3.458
4		4.133
4.5		4.833
5		5.542

Table 3.2 Ar-$^{15}N_2$ solid solutions with different concentrations: Impurity component of heat capacity (Joules/kelvin).

T	0.131mol%	0.25mol%
.5	2.815	1.907
.6	2.382	2.744
.7	3.030	3.325
.8	3.920	3.539
.9	4.248	3.808
1.0	4.112	3.897
1.1	3.905	3.860
1.2	3.715	
1.3	4.176	3.722
1.4	3.745	3.633
1.6	3.824	3.252
1.7	2.905	
1.8	2.994	3.020
1.9	2.192	2.800
2.0		2.557
2.5		2.369
3.0	2.966	2.940
3.5		2.872
4.0		3.471
4.5		3.149
5.0		4.693

Table 3.3.Kr-$^{14}N_2$ solid solutions with different concentrations, impurity component of heat capacity (Joules/mole kelvin):

3.2 DATA ANALYSIS AND FINDINGS.

In the theoretical explanation of the rotational heat capacity of diatomic molecules on the basis of DMM model, the effective rotational constant B, and the renormalized potential parameter K are not readily available from theory, therefore B and K are used as adjustable parameters to fit experimental data.

The adjustment of these parameters is done using the computer program shown in appendix A. After selecting the values of K and B roughly a fine adjustment to the best fit is obtained using the procedure that follw.

3.2.1 procedure.

1) The eigen values of the energy levels of the Devonshira spectrun computed by Sauer[12], are taken.
2) a. The height of all levels above the A_{1g} level is calculated at knowen values of K, and the curve representing these points is approximated pollynomially.
   b. The same is done as in step 2a for levels corresponding to untisymmetric levels above the T_{1u} level.

The spectrum obtained in step 2a) is used to compute the heat capacity with the assumption there is conversion between the different spin species, and the spectrum obtained in 2b) is used to compute the heat capacity with the assumption the high

temperature composition of the spin modifications is frozen at low temperatures.

3) Having the spectra for the two assumptions and for continuous values of K, a computer is programmed to set experimental points; compute and plot the heat capacity curves using equation 2.7a (or equation 7b for the heavier isotope of nitrogen) for the spectra in steps 2a and 2b separately all on the same window (see appendix A).

This enable to draw the theoretically calculated curves and the experimental points on the same plane so that the fit of the curve is easily seen. The parameters that best agree with the experimental points are selected, and the follwing conclusions are drawn.

3.2.2 Conversion.

For all choices of B and K, that agree the "hightemperature" exprimental points, the peak predicted by the theory according to the spectrum in step 2a (assumption there is conversion) is found to be two to three times greater in magnitude than the peak observed on the smoothed experimental result.

This gave us a reason to conclude that conversion between the spin modifactions of nitrogen molecules, trapped in Ar and Kr, could not occur. That is the high temperature composition

of the two species is retained down to 0.5k. Even if there is conversion the time required must be very very much longer than the duration of measuring the heat capacity (approximately 1hr.)

The case of Ar-$^{15}N_2$ solid solutions lead to the same conclusions. This shows that **conversion is independent of the nuclear spin** of the molecule under consideration.

One of such observations, for $^{14}N_2$ in Ar: 0.25mole% is illustrated in fig 3.4.

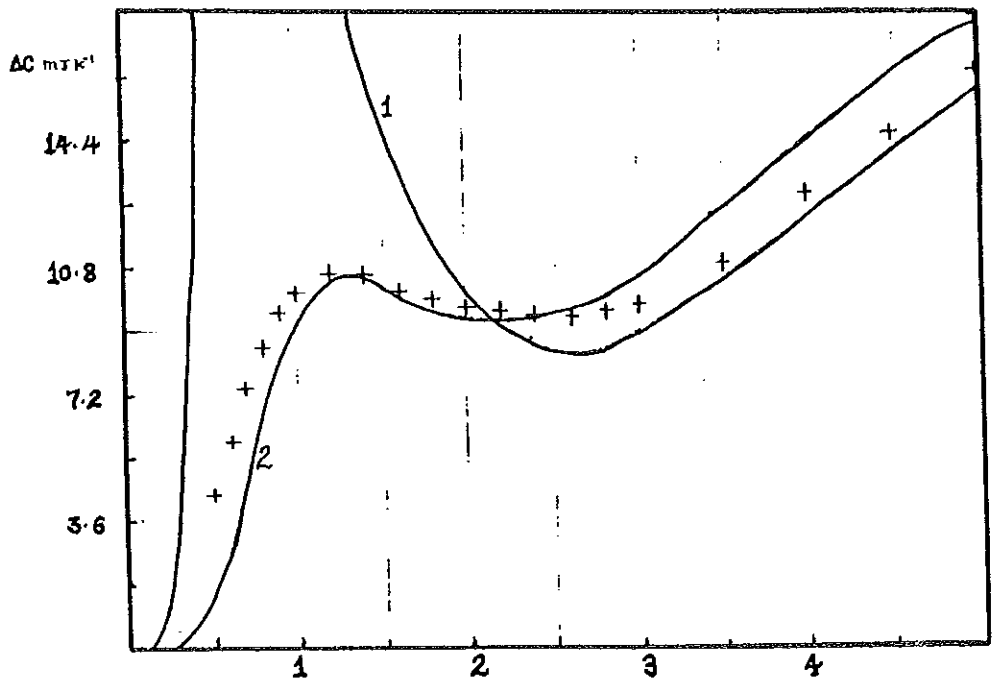

Fig 3.4. Ar-$^{14}N_2$,0.25mole% impurity +) experimental points curve 1) assuminng there is conversion and 2) assuming there is no conversion for E = 14.11 and B=1.50.

The problem of conversion is now settled, in the subsequent analysis we therefore assume frozen high temperature composition only.

3.2.3 Topography of the potential.

All attempts to obtain a fit between the experiment and the theory using negative values of **K** did not agree with the experiment around the observed experimental low temperature peak. The problem in this case is not the size of the peak but its position with respect to temperature. The theoretical peak is positioned below 0.5k and the theoretical heat capacity for temperatures below the position of the experimental peak is higher than the expermental heat capacity for all parameters that fit above 2k.

The grater heat capacity predicted by the theory for negative values of **K** is the most serious drawback for it implies higher density of states than the density of states implied by the measured heat capacity data. If one tries to modify the spectrum coresspnding to negative values of **K**, some of the levels should be compressed together so as to decrease the density of states and lower the predicted heat capacity. But this amounts lowering the symmetry of crystal field, whch is impossible since the octahedral symmetry already used posses the lowest possible symmetry in three dimensions.

Therefore prefference should be given to a model with K > 0, and we can conclude the equilibrium orientation of nitrogen molecules in Ar and Kr is along the <100> directions. This result is in agreement with the calculation of Manz and Mirsky [7], for CO molecules.

The two ambiguities that were kept under question from the results of high temperature measurements are now cleared. The detailes of the analysis for positive K and hightemperature composition nuclear spin-modification, leading to the ultimate taste of the DMM model itself is presented in what follows.

3.2.4 Varying parameters B and K : $0 \leq B \leq B_o ; K > 0$

Varying B for a given value of K is rescaling the spectrum shown in fig 2.3. ie. increasing B amounts widening the gap between any two levels, this is seen by the lowered heat capacity for the calculated curves in fig 3.5 (curves 1,2 and 3). The curves will tend to the Devonshire's model heat capacity curve when B approaches B_0.

Varying K, which characterizes the depth of the interaction potential between the impurity and the crystal field, for a fixed B is equivalent to view the spectrum from different points on the K-axis in fig 2.3. As K increses from zero the spectrum changes from that of a free rotor to a librator spectrum via hindered rotor spectrum for intermediate

values of K, this is seen by the decrease in heat capacity as K is increased : curves 4,5 and 6 of fig 3.5.

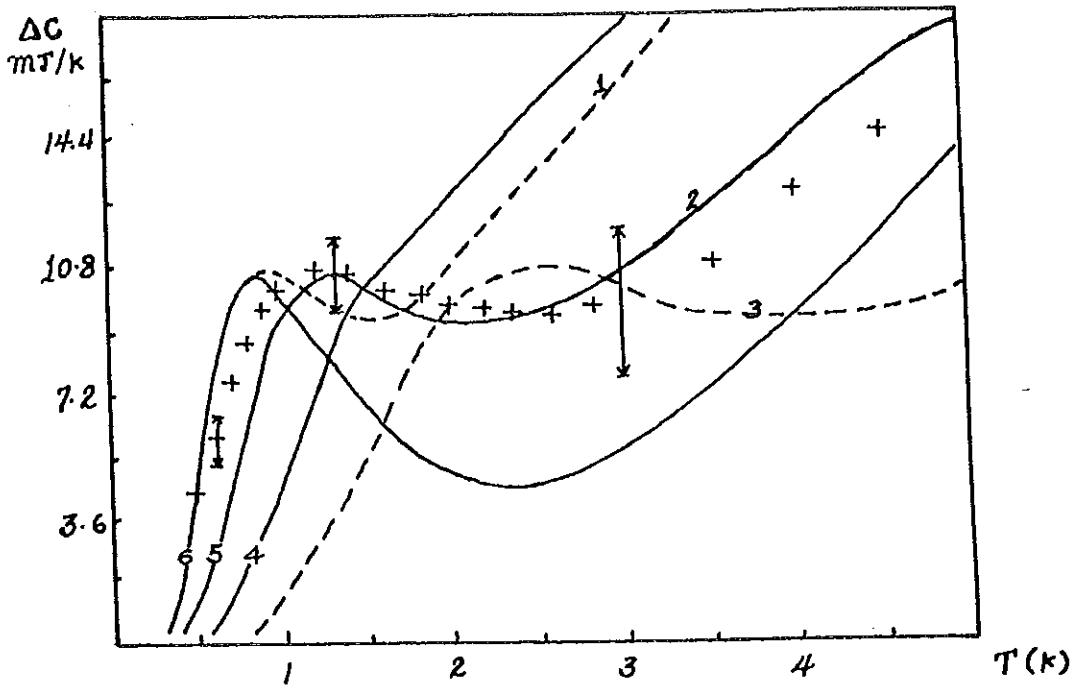

Fig 3.5 Changing B for fixed value of K = 14.11 curve 1) B=1.00; 2) B=1.50; 3) B=2.88 and changing K for fixed value of B=1.50: curve 4) K=10; 5) K=14.11; 6) K=18.00.

3.2.5. Determination of B and K

Following the procedure of analysis developed so far, we proceed to determine B and K for $^{14}N_2$ and $^{15}N_2$ in Ar and Kr, that best agree with experimental points.

(i) Ar-$^{14}N_2$ Solid solutions.

Agreement between the experimental points and the DMM theory is achieved for B=1.50 and K=14.11.

The reduced excess heat capacity of the solutions is seen to be independent of concentration for n≥0.25mol%. This shows, the importance of impurity-impurity interaction for higher concentrations. In the DMM theory, the dynamic interaction between the impurities is not taken in to account therefore, the fitting parameters K and B are selected for concentrations for which the reduced excess heat capacity is independent of the concentration n.

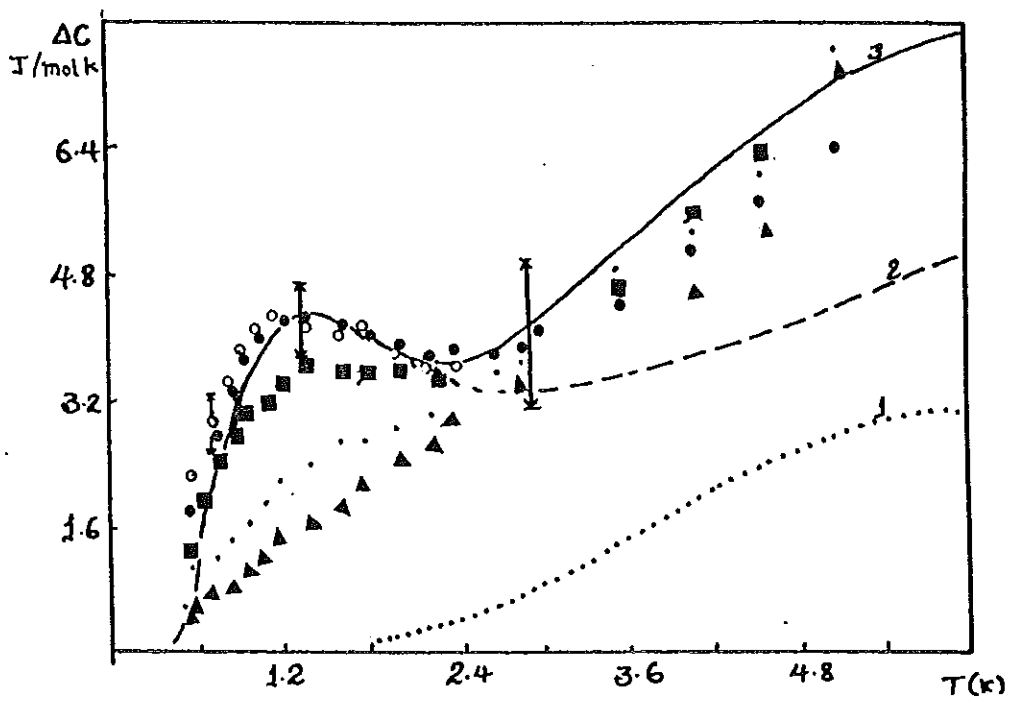

Fig 3.6 Temperature dependence of the reduced excess heat capacity Δ C (normalized to the impurity concentration n) for solid solutions of $^{14}N_2$ in Ar. Experimental points, ⊙) 0.12mole% ·) 1.02mole% ○) 0.25mole% ▲) 2.74mole% ■) 0.50mole% Calculations DMM model, curve 1) $\frac{1}{3}\Delta C_u$, 2) $\frac{2}{3}\Delta C_g$, 3)

At the lowest temperatures the heat capacity is predominantly from the ortho-species. This is to be expected since the gap between A_{1g} (J=0) and E_g (J=2) levels is much smaller than the gap between T_{1u} (J=1) and T_{1u} (J=3) levels, which makes molecules that populate the A_{1g} level to be excited easily when heat is added to the system and hence contribute to the heat capacity. In addition to this factor the molecules occupying the symmetric energy states are the majorities ie 2/3 of the total impurities always find themselves occupying symmetric energy states.

Figure 3.6 shows that the DMM model can not provide a quantitative description of the experimental results for temperatures lower than the position of the lowtemperature peak.

(ii) Ar-$^{15}N_2$ Solid solutions.

The heavier isotope of nitrogen is quite different from the lighter one, in that only 1/4 of the total molecules are characterized by symmetric wave functions in the case of $^{15}N_2$ and the nuclei constituting the heavier molecule are Fermi particles.

Analysis of the heat capacity data of the heavier isotope in Ar is in view of possible dependence of the energy spectrum on these differences.

Calculations in the frame work of DMM model provide no better curve, which is close to the experimental points, than shown in fig 3.7.

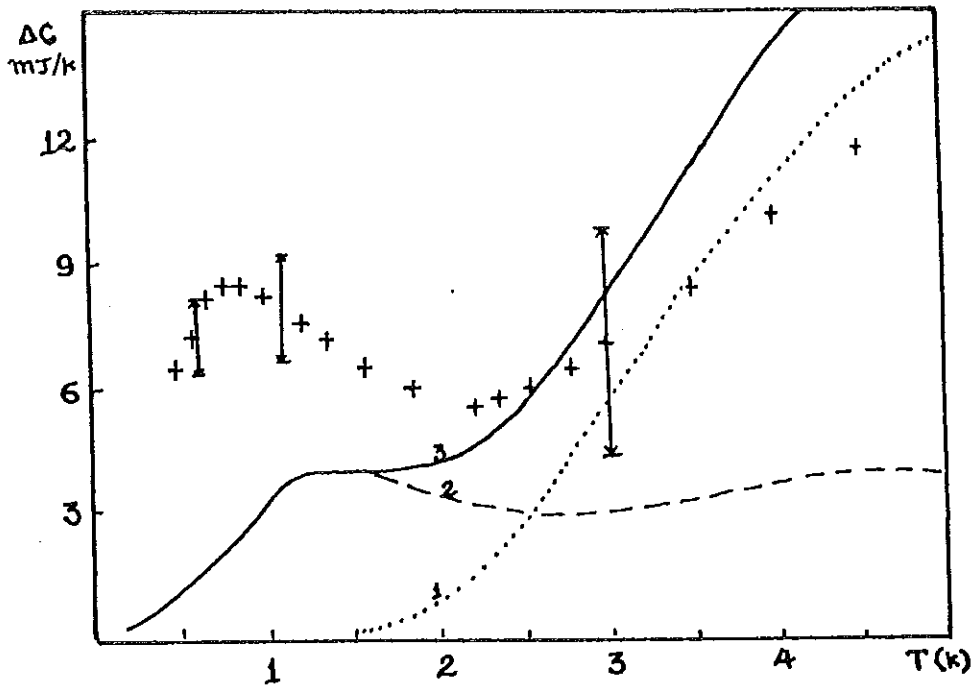

Fig 3.7 Temperature dependence of the impurity component of heat capacity for solid solutions of $^{15}N_2$ in Ar. Experimental points, +) 0.24 mole% Calculations DMM model: curves 1) $\frac{3}{4}\Delta C_u$ 2) $\frac{1}{4}\Delta C_g$

3) $\frac{1}{4}\Delta C_g + \frac{3}{4}\Delta C_u$

As can be seen from fig 3.7, there is much difference between the theoretical curve and the experimental points specially below 2k. The heat capacity predicted by the theory is far below from what is observed as compared with the case of

$^{14}N_2$, this is explainable from the models view point ie only a quarter of the total molecules occupy the symmetric states which are dominant heat capacity contributors in this temperature region. This shows the apparently slight deviation from experimental points in the case of $^{14}N_2$, for temperatures below the position of the low temperature peak, is serious for $^{15}N_2$ to the extent that the model fail to describe low temperature experimental points even qualitatively.

Therefore $^{15}N_2$ is more promising for the study of low lying energy spectrum, compared with $^{14}N_2$ by heat capacity method.

(iii) Kr-$^{14}N_2$ Solid solutions.

The lattice spacing being greater in Kr than in Ar, we expect that a given $^{14}N_2$ molecule trapped in Kr, has less interaction potential with the host lattice, compared with Ar. Therefore the barrier for rotation would be smaller and as the result the rotational constant of $^{14}N_2$ in Kr would be greater. This expectation is in accord with theoretical calculations [2].

Analysis of the data shows, the best fit with experimental result is obtained for B=1.75 and K=16.37.

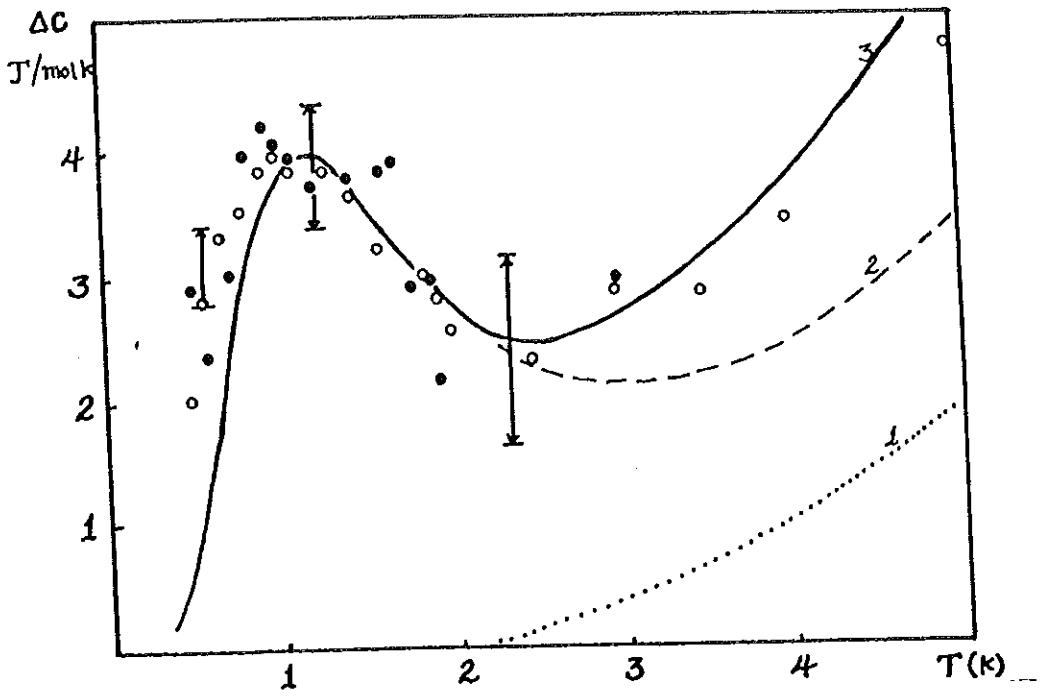

Fig 3.8 Temperature dependence of the impurity component of heat capacity (normalized to impurity concentration n) for solid solutions of $^{14}N_2$ in Kr. Experimental points, ●) 0.131 mole% ○)0.25 mole%

Calculations DFH model, curves: 1) $\frac{1}{3}\Delta C_u$ 2) $\frac{2}{3}\Delta C_g$ 3) $\frac{2}{3}\Delta C_g+\frac{1}{3}\Delta C_u$

The value of B is up to our expectation, ie it is greater in Kr than in Ar, but experimental fit shows that our expectation regarding K is not correct. K is even greater in Kr than in Ar. The possible explanation of this phenomena lies on the high polarizability of Kr atoms as compared with Ar atoms which results in greater dispersion interaction between $^{14}N_2$ and Kr atoms so that the impurity feels stronger crystal field as the result of which the rotation is more hindered. This enables us

to conclude that the theoretical predictions regarding K values could not always survive experimental tests. The fit for Kr-$^{14}N_2$ solutions could not explain experimental points qualitatively at the lowest temperatures.

CHAPTER IV MODIFICATION OF THE DMM SPECTRUM AND CONCLUSIONS.

4.1 INTRODUCTION

It was pointed out in the previous chapter that the famed DMM model, which in the final analysis counts on the Devonshire spectrum by way of renormalizing the rotational constant and the magnitude of the crystal field, does not provide a quantitative description of experimental observations.

In the DMM theory it is argued that the cubic symmetry of the field is restored due to the instantaneous spatial adjustment of the matrix atoms surrounding the impurity, and hence the Devonshire spectrum can be used for the best fitting renormalized parameters. The model agrees very well in high temperature measurements of heat capacity where higher energy levels, which are less sensitive to the details of the dynamics of the impurities are mainly involved.

Here it seems reasonable to question: is there no limit to this assumption?. i.e. if measurements in the high temperature regions are in agreement with the assumption, to confirm preservation of symmetrty, does this give any clue as to the

validity of the assumption for all parts of the spectrum specially the lowest ones. There appear no reason to stick on this assumption as long as this part of the model is hardly tenable theoretically except experimental justifications like heat capacity and thermal expansion measurements at higher temperatures.

Other factors like conversion; interaction between impurity molecules could not be responsible for the observed discrepancy since conversion produces strong contribution and interaction is out of question since the theory itself ignores this factor.

4.2 Findings and comparison with the experiment.

It is seen from figs. 3.6, 3.7 and 3.8 that at lowest temperatures of the observation theory gave less amount of heat capacity than the experiment. This suggests the existence of denser energy states than used in the theory.

It is infact the low-lying levels A_{1g}, T_{1u} and E_g predominantly populated below T<1.4K. These close low-energy levels are separated from the other part of the spectrum by an energy gap $\Delta E \sim 8B$ The heat capacity observed in the temperature region, where the calculated heat capacity curve fail to agree with experimental points, is mainly contributed from the low lying levels. This gave a us clue that, if the

real density of states is higher than predicted in the theory, there must be a split of the degenerate T_{1u} and E_g levels so that the theoretical heat capacity is elevated to fit experimental points.

The DMM spectrum was first calculated by using the parameters that gave good fit in the high temperature region (B and K obtained in sec.3.2). The split of T_{1u} and E_g levels is introduced in the spectrum keeping the center of gravity of the levels. The heat capacity is then computed for different split gaps until the best agreement is achieved with the experimental values.

Following this porcedure the experimental values of ΔC for all solutions under consideration are correctly described by the modified DMM model in which T_{1u} and E_g are splitted.

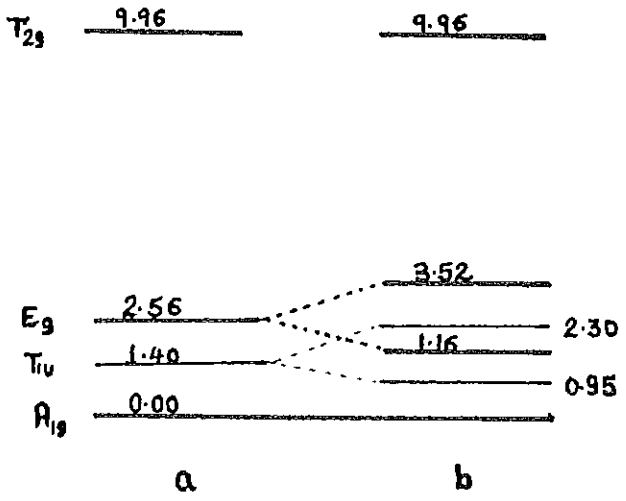

Fig 4.1 The low-energy part of the spectrum of $^{14}N_2$ molecule in Ar.(the energy values are in kelvin). (a) rotational spectrum of DMM model. (b) the modified spectrum

The theoretical calculations using the modified spectrum together with experimental points is shown in fig 4.2a.

The modified spectrum that gives the best fit for $Ar-^{14}N_2$ is also the best for $Ar-_{15}N_2$ solution. The sucess of the modified spectrum for the heavier isootope of nitrogen unlike the DMM model justifies the validity of our assumption regarding the lowest part of the spectrum and shows that the rotational spectrum is independent of the type of the nuclei constituting the molecules.

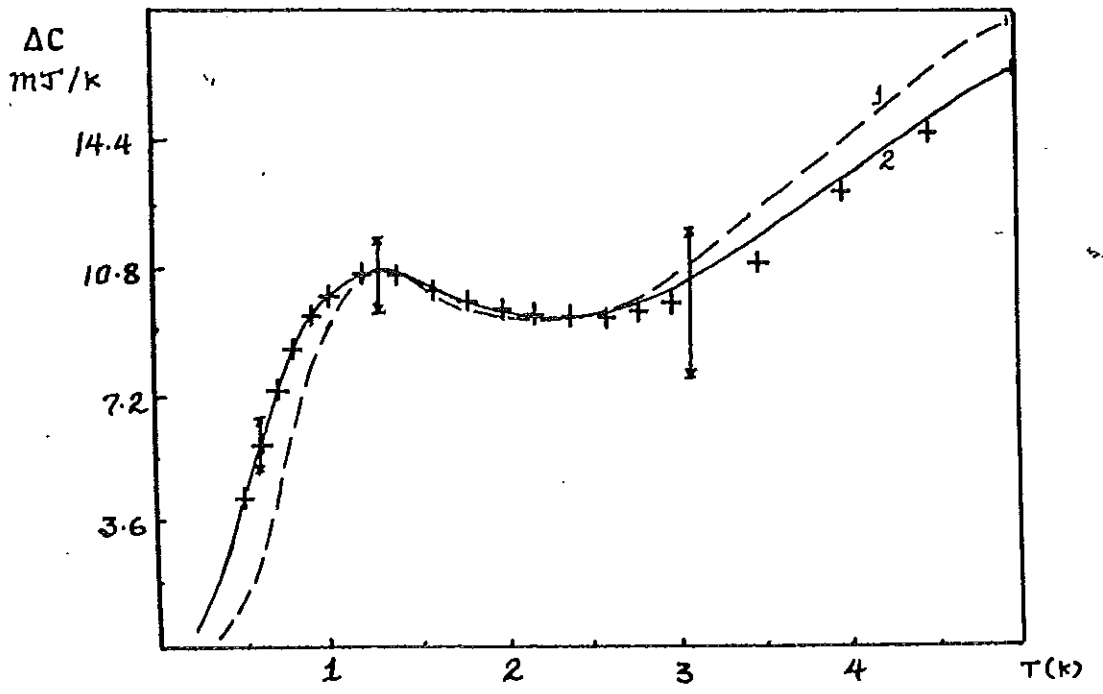

a

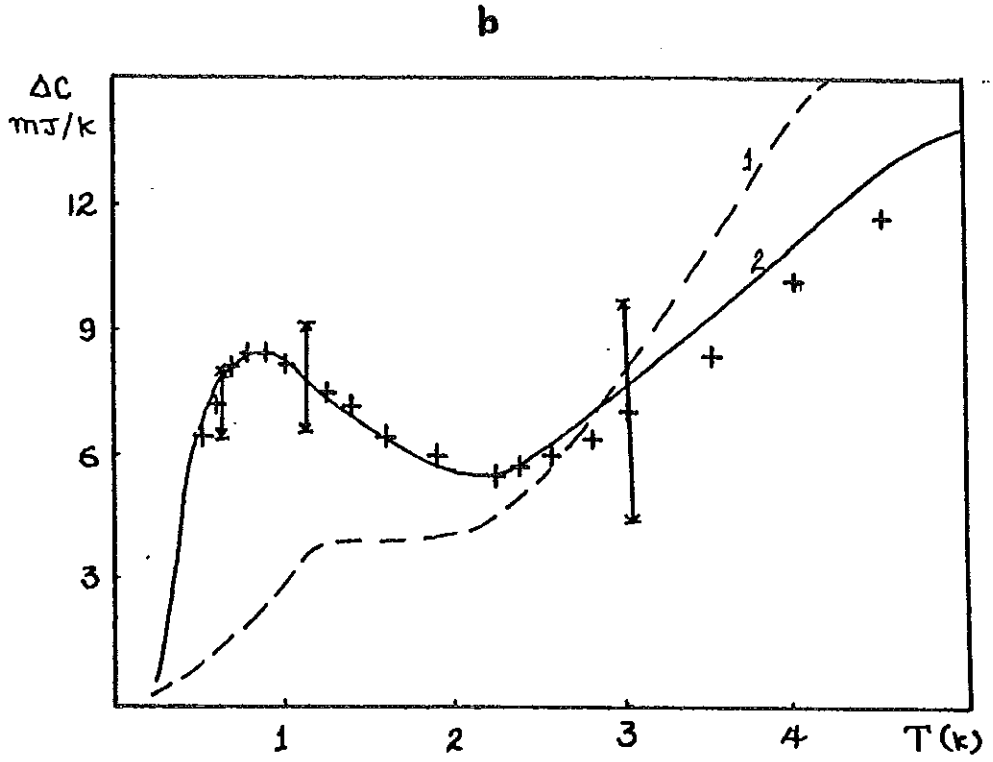

Fig 4.2 Temperature dependence of the reduced excess heat capacity : +) experimental points. (a) Ar-$^{14}N_2$, 0.25 mole% b) Ar-$^{15}N_2$, 0.24 mole% . Calculation 1) calculation by DRM spectrum 2) calculation by the modified spectrum.

The DMM model spectrum and splitting of the two lowest levels providing the best fit with the values of ΔC in Kr-$^{14}N_2$ solid solutions is presented in Fig. 4.3.

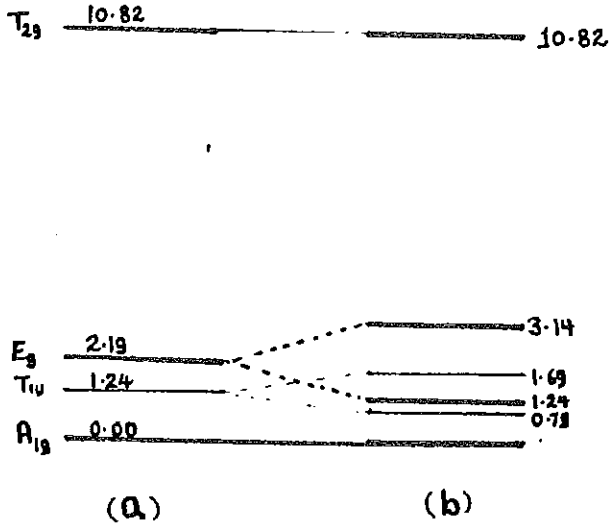

Fig 4.3 The low-energy part of the spectrum of $^{14}N_2$ molecules in Kr.(a) rotational spectrum of DMM model. (b) rotational spectrum of DMM model in which T_{1u} and E_g levels are splitted.

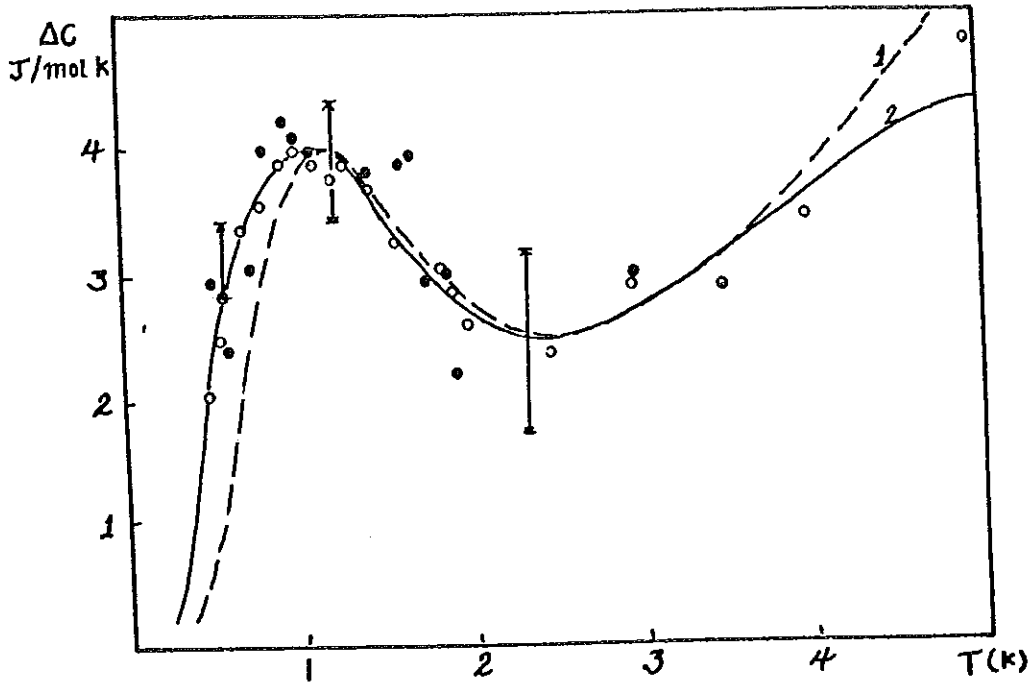

Fig 4.4 Temperature dependence of the reduced excess heat capacity of $^{14}N_2$ in Kr. EXPERIMENT e) 0.13 mole% $^{14}N_2$,o) 0.25 mole% $^{14}N_2$ THEORY curve 1) calculation by DMM model spectrum 2) calculation using the modified spectrum

4.3 SUMMARY AND CONCLUSIONS

The applicability of the DMM model is limited for those concentrations that the direct or indirect impurity-impurity interaction is negligible. The experimental reduced excess heat capacity is independent of concentration for concentrations $n \leq 0.25 mol\%$. Therefore determination of the renormalized parameters must be in comparison with experimental results

with concentrations lower than 0.25mole%.

Based on the results of previous work [2] and the present analysis we conclude that the high temperature composition of the different spin species of nitrogen remain unchanged down to 0.5 kelvin and conversion is independent of the nuclear spin.

The equilibrium orientations of N_2 molecules is along the <100> directions of the crystal. This conclusion is drawn from the failure of the negative part of the spectrum to fit experimental heat capacity measurements.

Calculations of the impurity component of the heat capacity within the frame work of the DMM model corrresponds to real situations for high-energy rotational spectrum, while the low energy rotational spectra does not. The difference in behavior between the calculated and experimental temperature dependence of ΔC, which is most significant in the low-temperature region, is associated with the extra splitting of the lowest rotational levels.

A quantitative agreement between the experimental values and theoretical ones in the framework of DMM model can be attained by assuming the splitting of lowest energy levels of the DMM model spectrum. Therefore the assumption of the DMM model that the symmetry of the field is preserved due to the instantaneous spatial adjustement of pseudo rotating cage is

not valid for the lowest part of the spectrum. The A_{1g} and T_{1u} levels are splitted in such a way that the center of gravity of the levels remain unchanged.

The success of the modified spectrum for both isotopes of nitrogen is belived to be additional justification for the validity of the assumption the low lying energy levels are splitted.

LIST OF REFERENCES

[1] Sumarkov V.V, Freiman Yu.A, Manzhelii V.G. and Popov V.A. ,Hindered rotation of linear molecules CO in solid Kr matrix,Sov Journal of low temperature physics,1988,V14,N11.

[2] Manzhelii V.G, etal., Hindered rotation of linear molecules in atomic cryocrystals and thermal properties of solutions, Sov.J.of Low Temp Phys.,1986,12,2.

[3] V.Narayanamurti and R.O.Pohl, Rev.Mod.Phys.,42 No 2, 1970.

[4] T.Yamamoto, Y.Kataoka, and K.Okada, Theory of phase transitions in solid methanes. J.Chem.phys. Vol 66, No 6, 1977

[5] K.Mendelsson, F.R.S.,CRYOPHYSICS,Interscience publishers, Inc.Newyork 1960.

[6] Manz J. Rotating Molecules Trapped in Pseudorotating cage, J. of the American chemical society, 1980 '102:6'.

[7] J. Manz and K. Mirsky ,The Geometry and vibrational frequency shift of CO molecules in Ar matrix studied by force field calculations., J.Chem Phys 46, 457 (1980).

[8] Devonshire A.F., The rotation of molecules in fields of octahedral symmetry, Proc.Roy.Soc. A-1936-153,N880.

[9] J.C. Burford and G.M. Graham., Specific heat anomaly in solidified Gases due to O_2 impurity, J.Chem phys. 1968, V49, 2.

[10] Finegold L., Low temperature heat capacities of solid Ar and Kr.,Phy.Rev, 1969, V177, No3.

[11] Bagatskii M.I., etal, Heat cpacity of solid parahydrogen, Sov J. of Low temperature physics., 1984, V10,#10.

[12] Saur P.,On hindered rotation of linear molecules, Z.phys 1966-194, No.4.

[13] C. Kittle introduction to Solid state physics.

APPENDICES

A Program to compute rotational heat capacity of $^{14}N_2$

```
10 REM"calculation of rotl. heat capacity DMM model"
20 INPUT "INPUT FILENAME ",F$
30 DIM E(10),Y(10),G(10)
40 OPEN "I",#1,F$
50 H=0
60 IF EOF(1) GOTO 80
70 INPUT #1,P,AEX:H=H+1:GOTO 60
80 CLOSE #1:PRINT H
90 DIM P(H):DIM AEX(H)
100 OPEN "I",#1,F$
110 FOR I=1 TO H
120 INPUT #1,P(I),AEX(I):GOSUB 2960
130 PRINT P(I),AEX(I):NEXT I:STOP
140 G=0
150 FOR I=1 TO H
160 IF AEX(I)>G THEN G=AEX(I)
170 NEXT I:PRINT G
180 REM "selection of parameters"
190 Y=G
200 P=0
210 Y=Y*10
220 P=P+1
230 IF INT(Y)=0 GOTO 210
240 SCREEN 9
250 VIEW
260 VIEW PRINT
270 CLS
280 KEY OFF
290 SCREEN 9:COLOR 1,2
300 Q=(1+INT(G*10^P))*10^(-P):LOCATE 23,1:PRINT "Q=";Q:BEEP
310 LOCATE 24,1:INPUT "INPUT windovs parameters - T1,A1,T2,A2
",T1,A1,T2,A2
320 VIEW (135,0)-(515,280),0
330 K1=4:FOR I=1 TO 5
340 LOCATE K1,11:B1$=".##^^^^":B1=A1+(A2-A1)*(10-2*I)/10:PRINT
USING B1$;B1
350 K1=K1+4
360  NEXT  I:LOCATE  1,1:PRINT  "(dA=";(A2-A1)/10;")":LOCATE
1,16:PRINT "A"
370 S1=15:FOR I=0 TO 4
380 LOCATE 21,S1:PRINT T1+I*(T2-T1)/5:S1=S1+10
390  NEXT  I:LOCATE  21,66:PRINT  "T":LOCATE  21,71:PRINT
"(dT=";(T2-T1)/10;")"
400 VIEW PRINT 22 TO 24
410 WINDOW (T1,A1)-(T2,A2)
420 FOR F=T1 TO T2+(T2-T1)/10 STEP (T2-T1)/10
430 LINE (F,A1)-(F,A2),1
```

```
440LINE(T1,A1+(A2-A1)*(F-T1)/(T2-T1))-(T2,A1+(A2-A1)*(F-T1)/(
T2-T1)),1
450 NEXT F
460 FOR I=1 TO H
470 LINE (P(I)-(T2-T1)*.01,AEX(I))-(P(I)+(T2-T1)*.01,AEX(I)),15
4       8       0                          L       I       N       E
(P(I),AEX(I)-.01*(A2-A1))-(P(I),AEX(I)+.01*(A2-A1)),15:GOTO 510
490 CIRCLE (P(I),AEX(I)),(T2-T1)*8.999999E-03,15:GOTO 510
500 CIRCLE (P(I),AEX(I)),(T2-T1)*4.999999E-03,15:GOTO 510
510 NEXT I
520 LOCATE 24,5:BEEP
530 PRINT "0-cont;1-change scale;2-curve"
540 K$=INKEY$:IF K$="" THEN GOTO 540
550 ON VAL(K$) GOTO 580,590
560 GOSUB 610
570 GOTO 520
580 GOTO 250
590 STOP:GOSUB 1370
600 GOTO 520
610 PRINT "delta C N2 (14) in  solid Ar or Kr"
620 GOTO 630
630 INPUT "concentration=?",X
640 K1=37.72:REM K1 - valentn.(K)
650 K2=-10.94:REM K2 - dispers.(K)
660 K3=-.44:REM K3 - mult.(K)
690 INPUT "start T=?",T3:INPUT "fin. T=?",T4
700 INPUT "step T=?",DT
710 INPUT "rot.const.in grad(K) =?  ",B
720 INPUT "const.k=? (K/B)",K
730 COL=8
750 A(1)=2:REM level N1 T1u
760 B(1)=.0170403
770 C(1)=-6.92721E-03
780 D(1)=2.22036E-04
790 F(1)=-2.16383E-06
800 A(2)=6:REM level N2 Eg
810 B(2)=-.3014313
820 C(2)=3.40012E-03
830 D(2)=6.97034E-05
840 F(2)=-1.34216E-06
850 A(3)=6:REM  level N3 T2g
860 B(3)=.1732634
870 C(3)=8.88508E-03
880 D(3)=-8.5783E-05
890 F(3)=-2.65833E-07
900 A(4)=12:REM level N4 A2u
910 B(4)=.34761
920 C(4)=.0111373
930 D(4)=-5.495E-05
940 F(4)=7.58333E-07
950 A(5)=12:REM level N5 T1u
960 B(5)=-.2351643
970 C(5)=.0230923
980 D(5)=-3.11891E-04
990 F(5)=1.00116E-06
1000 A(6)=12:REM level N6 T2u
```

```
1010 B(6)=.0426594
1020 C(6)=9.95126E-03
1030 D(6)=-1.0299E-04
1040 F(6)=4.31666E-08
1050 A(7)=20:REM level N7 A1g
1060 B(7)=-.2859573
1070 C(7)=.019511
1080 D(7)=2.40136E-04
1090 F(7)=-1.594E-06
1100 A(8)=20:REM level N8 Eg
1110 B(8)=-.052688
1120 C(8)=.0164983
1130 D(8)=-1.3855E-04
1140 F(8)=-5.38333E-08
1150 A(9)=20:REM level N9 T1g
1160 B(9)=-.13315116#
1170 C(9)=7.31807E-03
1180 D(9)=3.11817E-05
1190 F(9)=-1.42216E-06
1200 A(10)=20:REM level N10 T2g
1210 B(10)=.2169632
1220 C(10)=.0123126
1230 D(10)=-6.372E-05
1240 F(10)=-7.55383E-07
1250 G(1)=3:REM T1u
1260 G(2)=2:REM Eg
1270 G(3)=3:REM T2g
1280 G(4)=1:REM A2u
1290 G(5)=3:REM T1u
1300 G(6)=3:REM T2u
1310 G(7)=1:REM A1g
1320 G(8)=2:REM Eg
1330 G(9)=3:REM T1g
1340 G(10)=3:REM T2g
1370 FOR J=1 TO 10
1380 E(J)=A(J)+B(J)*K+C(J)*K^2+D(J)*K^3+F(J)*K^4
1430 NEXT J
1440 FOR T=T3 TO T4 STEP DT:T=T/B
1450 J=10
1460 A=0:Z=0:E(0)=0:G(0)=1:Y(0)=0:REM E(0),G(0),Y(0)-0level A1g
1470 FOR I=0 TO J:A=G(I)*EXP(-E(I)/T):Z=Z+A:NEXT I
1480 A=0:EC=0
1490  FOR  I=0  TO  J:A=G(I)*E(I)*EXP(-E(I)/T):EC=EC+A:NEXT
I:EC=EC/Z
1550 A=0:E2C=0
1560  FOR  I=0  TO  J:A=G(I)*E(I)^2*EXP(-E(I)/T):E2C=E2C+A:NEXT
I:E2C=E2C/Z
1570 A=0:E=0
1590  E2=E2C-EC^2:E2=E2*X*8.3144/(T*T)
1630 T=T*B
1650 PSET(T,E2),COL:NEXT T
1660 COLG=6
1675 FOR T=T3 TO T4 STEP DT
1680 A(1)=6:REM level N2 Eg
1690 B(1)=-.3014313
1700 C(1)=3.40012E-03
```

```
1710 D(1)=0!
1720 F(1)=-1.34216E-06
1730 A(2)=6:REM  level N3 T2g
1740 B(2)=.1732634
1750 C(2)=8.88508E-03
1760 D(2)=-8.5783E-05
1770 F(2)=-2.65833E-07
1780 A(3)=20:REM level N7 A1g
1790 B(3)=-.2859573
1800 C(3)=.019511
1810 D(3)=2.40136E-04
1820 F(3)=-1.594E-06
1830 A(4)=20:REM level N8 Eg
1840 B(4)=-.052688
1850 C(4)=.0164983
1860 D(4)=-1.3855E-04
1870 F(4)=-5.38333E-08
1880 A(5)=20:REM level N9 T1g
1890 B(5)=-.1331516
1900 C(5)=7.31807E-03
1910 D(5)=3.11817E-05
1920 F(5)=-1.42216E-06
1930 A(6)=20:REM level N10 T2g
1940 B(6)=.2169632
1950 C(6)=.0123126
1960 D(6)=-6.372E-05
1970 F(6)=-7.55383E-07
1980 G(1)=2:REM Eg
1990 G(2)=3:REM T2g
2000 G(3)=1:REM A1g
2010 G(4)=2:REM Eg
2020 G(5)=3:REM T1g
2030 G(6)=3:REM T2g
2060 FOR J=1 TO 6
2070 E(J)=A(J)+B(J)*K+C(J)*K^2+D(J)*K^3+F(J)*K^4
2120 NEXT J
2130 T=T/B
2140 J=6
2150 A=0:Z=0:E(0)=0:G(0)=1:Y(0)=0:REM E(0),G(0),Y(0)-0level A1g
2160 FOR I=0 TO J:A=G(I)*EXP(-E(I)/T):Z=Z+A:NEXT I
2170 A=0:EC=0
2180  FOR  I=0  TO  J:A=G(I)*E(I)*EXP(-E(I)/T):EC=EC+A:NEXT
I:EC=EC/Z
2240 A=0:E2C=0
2250  FOR  I=0  TO  J:A=G(I)*E(I)^2*EXP(-E(I)/T):E2C=E2C+A:NEXT
I:E2C=E2C/Z
2260 A=0:E=0
2280 E2=E2C-EC^2:E2=.6666*E2*X*8.3144/(T*T)
2320 T=T*B
2330 ALPHAG=E2:REM g-levels
2340 COLU=11
2360 A(1)=10:REM level N5 T1u
2370 B(1)=-.252208
2380 C(1)=.03002
2390 D(1)=-5.33955E-04
2400 F(1)=3.16533E-06
```

B program to select the splitting parameters that provide best fit with experimental points.

```
10 REM"to select splitting parameters for 14N2 in Ar."
20 INPUT "INPUT FILENAME ",F$
30 DIM E(10),Y(10),G(10)
40 OPEN "I",#1,F$
50 H=0
60 IF EOF(1) GOTO 80
70 INPUT #1,P,AEX:H=H+1:GOTO 60
80 CLOSE #1:PRINT H
90 DIM P(H):DIM AEX(H)
100 OPEN "I",#1,F$
110 FOR I=1 TO H
120 INPUT #1,P(I),AEX(I):GOSUB 1310
130 PRINT P(I),AEX(I):NEXT I:STOP
140 G=0
150 FOR I=1 TO H
160 IF AEX(I)>G THEN G=AEX(I)
170 NEXT I:PRINT G
190 Y=G
200 P=0
210 Y=Y*10
220 P=P+1
230 IF INT(Y)=0 GOTO 210
240 SCREEN 9
250 VIEW
260 VIEW PRINT
270 CLS
280 KEY OFF
290 SCREEN 9:COLOR 1,2
300 Q=(1+INT(G*10^P))*10^(-P):LOCATE 23,1:PRINT "Q=";Q:BEEP
310 LOCATE 24,1:INPUT "INPUT windovs parameters - T1,A1,T2,A2
",T1,A1,T2,A2
320 VIEW (135,0)-(515,280),0
330 K1=4:FOR I=1 TO 5
340 LOCATE K1,11:B1$=".##^^^^":B1=A1+(A2-A1)*(10-2*I)/10:PRINT
USING B1$;B1
350 K1=K1+4
360  NEXT  I:LOCATE  1,1:PRINT  "(dA=";(A2-A1)/10;")":LOCATE
1,16:PRINT "A"
370 S1=15:FOR I=0 TO 4
380 LOCATE 21,S1:PRINT T1+I*(T2-T1)/5:S1=S1+10
390  NEXT  I:LOCATE  21,66:PRINT  "T":LOCATE  21,71:PRINT
"(dT=";(T2-T1)/10;")"
400 VIEW PRINT 22 TO 24
410 WINDOW (T1,A1)-(T2,A2)
420 FOR F=T1 TO T2+(T2-T1)/10 STEP (T2-T1)/10
430 LINE (F,A1)-(F,A2),1
4                                4                                0
LINE(T1,A1+(A2-A1)*(F-T1)/(T2-T1))-(T2,A1+(A2-A1)*(F-T1)/(T2-
T1)),1
450 NEXT F
460 FOR I=1 TO H
470 LINE (P(I)-(T2-T1)*.01,AEX(I))-(P(I)+(T2-T1)*.01,AEX(I)),15
4       8       0                        L       I       N       E
```

```
(P(I),AEX(I)-.01*(A2-A1))-(P(I),AEX(I)+.01*(A2-A1)),15:GOTO 510
490 CIRCLE (P(I),AEX(I)),(T2-T1)*8.999999E-03,15:GOTO 510
500 CIRCLE (P(I),AEX(I)),(T2-T1)*4.999999E-03,15:GOTO 510
510 NEXT I
520 LOCATE 24,5:BEEP
530 PRINT "0-cont;1-change scale;2-curve"
540 K$=INKEY$:IF K$="" THEN GOTO 540
550 ON VAL(K$) GOTO 580,590
560 GOSUB 610
570 GOTO 520
580 GOTO 250
590 STOP:GOSUB 1370
600 GOTO 520
610 PRINT "delta C N2 (14) in  solid Ar or Kr"
620 GOTO 630
630 INPUT "concentration=?",X
660 K3=-.44:REM K3 - mult.(K)
690 INPUT "start T=?",T3:INPUT "fin. T=?",T4
700 INPUT "step T=?",DT
710 INPUT "rot.const.in grad(K) =?  ",B
715 INPUT "delta E for T1u u=?",U
720 INPUT "Input delta E for Eg g=?",G
730 COLG=7
740 FOR T=T3 TO T4 STEP DT
750 E(1)=2.5663514#-G
760 E(2)=2.5663514#+G
770 E(3)=9.9621718#
780 E(4)=20.460812#
790 E(5)=22.149906#
800 E(6)=19.609425#
810 E(7)=25.303746#
820 G(1)=1 :REM SPLITTED Eg level
830 G(2)=1
840 G(3)=3
850 G(4)=1
860 G(5)=2
870 G(6)=3
880 G(7)=3
900 T=T/B
920 A=0:Z=0:E(0)=0:G(0)=1:Y(0)=0:REM E(0),G(0),Y(0)-0level A1g
930 FOR I=0 TO 7:A=G(I)*EXP(-E(I)/T):Z=Z+A:NEXT I
940 A=0:EC=0
950  FOR  I=0  TO  7:A=G(I)*E(I)*EXP(-E(I)/T):EC=EC+A:NEXT
I:EC=EC/Z
960 A=0:E2C=0
970  FOR  I=0  TO  7:A=G(I)*E(I)^2*EXP(-E(I)/T):E2C=E2C+A:NEXT
I:E2C=E2C/Z
980 A=0:E=0
990 E2=E2C-EC^2:E2=.6666*E2*X*8.3144/(T*T)
1000 T=T*B
1010 ALPHAG=E2:REM g-levels
1020 COLU=11
1030 E(1)= 3*U
1040 E(2)=11.04357+U
1050 E(3)=12.808773#+U
1060 E(4)=17.538442#+U
```